Medicinal Chemistry Research (2025) 34:1695–1713
https://doi.org/10.1007/s00044-025-03434-0

MEDICINAL CHEMISTRY RESEARCH

ORIGINAL RESEARCH ARTICLE

Dual-PROTACs based on natural product derivative potassium dehydrographolide succinate: design, synthesis, and antitumor activity of a novel EGFR degrader

Ruling Shi[1] · Peixi Zhang[2] · Ming Chen[2] · Weiming Lu[2] · Meng Xu[2] · Huagong Zeng[2] · Jie He[2] · Yan Wang[2] · Yirong Lin[2] · Jieqing Liu[1]

Received: 4 April 2025 / Accepted: 10 June 2025 / Published online: 30 June 2025
© The Author(s), under exclusive licence to Springer Science+Business Media, LLC, part of Springer Nature 2025

Abstract

The epidermal growth factor receptor (EGFR) is overexpressed in various cancers and contributes to tumor progression and therapeutic resistance. Although EGFR-targeting small-molecule inhibitors are clinically available, their limited efficacy and acquired resistance pose major challenges. In this study, we designed and synthesized a novel class of dual proteolysis-targeting chimeras (PROTACs) incorporating the natural product derivative Potassium Dehydroandrographolide Succinate (PDS) as the protein of interest (POI) ligand. PDS was selected as the POI ligand due to its structural similarity to andrographolide, a natural compound known to inhibit EGFR signaling, suggesting that PDS may retain EGFR-binding potential despite lacking direct anti-tumor reports. Unlike conventional PROTACs, these molecules feature two CRBN E3 ligase ligands symmetrically attached via distinct linkers, thereby enhancing the likelihood of ternary complex formation and promoting more efficient EGFR degradation. Among the synthesized compounds, DP6 exhibited the most potent anti-proliferative activity in MCF-7 cells, with a 3.8-fold improvement over the parent PDS molecule. Western blotting confirmed that DP6 induced concentration-dependent EGFR degradation via the ubiquitin–proteasome system, suppressed downstream JAK2-STAT3 signaling, and promoted apoptosis. This study not only demonstrates the feasibility of utilizing structurally modified natural products as POI ligands, but also introduces a unique dual-ligand PROTAC architecture that may provide enhanced degradation potency for traditionally "undruggable" targets.

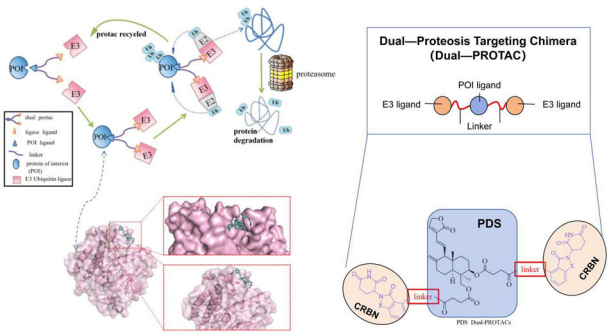

These authors contributed equally: Ruling Shi, Peixi Zhang.

✉ Jieqing Liu
liujieqing@hqu.edu.cn

[1] Department of Pharmacy, Quanzhou Medical College, Quanzhou, China

[2] Engineering Research Centre of Molecular Medicine of Ministry of Education, Key Laboratory of Fujian Molecular Medicine, Key Laboratory of Precision Medicine and Molecular Diagnosis of Fujian Universities, Key Laboratory of Xiamen Marine and Gene Drugs, School of Medicine, Huaqiao University, Quanzhou, P. R. China

Keywords Natural products · Proteolysis targeting chimeras (PROTAC) · Potassium dehydrographolide succinate(PDS) · EGFR · Antitumor

Introduction

Cancer is a disease characterized by the uncontrolled proliferation and migration of cells. The spectrum of therapeutic modalities available for cancer includes surgery, chemotherapy, radiation therapy, administration of anticancer medications, immunotherapy, and stem cell therapy [1]. Despite continuous advancements in treatment methodologies, cancer-related mortality has been increasing. According to research statistics from the National Cancer Centre, 2,574,200 new cancer deaths were reported in China in 2022. With China's aging population, it is anticipated that cancer will exert a profound impact on the national economy and societal development [2].

Recent advancements in targeted therapy have rendered it an effective treatment option for cancer patients [3]. These therapies, which rely on optimizing the binding affinity of drugs, operate on an 'occupancy-driven' mechanism of action. However, this mechanism limits the number of druggable targets and is associated with challenges such as drug resistance, short half-life, and off-target effects [4]. In contrast to small-molecule inhibitors and antibodies, PROTACs constitute a novel class of therapeutic agents that selectively facilitate the degradation of target proteins via endogenous protease systems, thus emerging as a significant and extensively discussed domain within the field of drug discovery over recent decades [5–9]. These molecules are heterobifunctional, comprising a ligand for the protein of interest (POI), a ligand for an E3 ubiquitin ligase, and a linker that connects the two ligands. This structure facilitates the recruitment of both the POI and the E3 ligase, forming a ternary complex ('E3-PROTAC-POI'), which leads to the degradation of the target protein through the ubiquitin-proteasome pathway [10].

Unlike traditional "occupancy-driven" inhibitors, (PROTACs employ an "event-driven" mechanism to induce the degradation of pathogenic proteins, thereby demonstrating superior efficacy and prolonged anti-tumor effects compared to mere inhibition of protein activity [11]. Furthermore, PROTACs facilitate efficient degradation with short reaction times, minimal catalytic quantities, and weak binding to target proteins, allowing for recycling and reduction of dose-related toxicity [5]. Additionally, PROTACs exhibit enhanced tolerability over small-molecule inhibitors in instances where target proteins are either mutated or expressed at low levels, and they possess a certain degree of tissue permeability, enabling action on intracellular targets [12]. As of March 2023, approximately 23 PROTAC molecular drugs have entered clinical research globally. In various PROTAC design approaches, Qi et al. selected the natural product ursolic acid as the protein of interest (POI) ligand and synthesized a series of PROTACs by designing and optimizing the linker in conjunction with thalidomide, thereby significantly enhancing the anti-tumor activity of ursolic acid [13]. It is thus hypothesized that the strategy of PROTAC could convert inactive or less active inhibitors derived from natural products into effective antitumor agents [14, 15].

Natural products serve as a rich source of lead compounds, offering unique chemical structures that provide a foundation for the synthesis or semi-synthesis of novel pharmaceuticals. Furthermore, their diverse biological activities render them invaluable in drug development. indicate that between 1981 and 2019, approximately two-thirds of small-molecule drugs were derived from natural products, with natural products and their derivatives accounting for around 70% of FDA-approved anti-cancer medications. Andrographolide (ADGL), a bicyclic diterpenoid lactone extracted from the natural plant Andrographis paniculata, exhibits a range of bioactivities, including anti-inflammatory, antibacterial, anti-tumor, anti-HIV, and immune-enhancing properties [16, 17]. Research has demonstrated that andrographolide targets the epidermal growth factor receptor (EGFR) to inhibit epithelial-mesenchymal transition during the early stages of cancer metastasis, thus exerting significant anti-tumor effects [18]. Nevertheless, its bioavailability is limited by its poor water solubility and low oral absorption.In order to improve its pharmacological properties,Potassium Dehydroandrographolide succinate (PDS) is a derivative obtained by structural modification of andrographolide (Fig. 1A). This compound exhibits immunomodulatory and notable anti-inflammatory efficacy and has been widely utilized in clinical settings. However, its anti-tumor activity remains unreported in the literature. ARQ-092 is an inhibitor that targets allosteric sites, and Yu et al. synthesized a carboxylic acid derivative by introducing three atoms into the phenyl ring structure on the left side of the molecule, subsequently employing it as a POI ligand to successfully generate a series of AKT-PROTAC degraders (Fig. 1B). Research findings indicate that the novel AKT PROTAC molecule 62 can induce significant degradation of AKT in the colon cancer cell line SW620 (Fig. 1C). These results suggest that lead compounds, following structural modification, can further enhance degradation efficiency against the original target protein through the PROTAC strategys

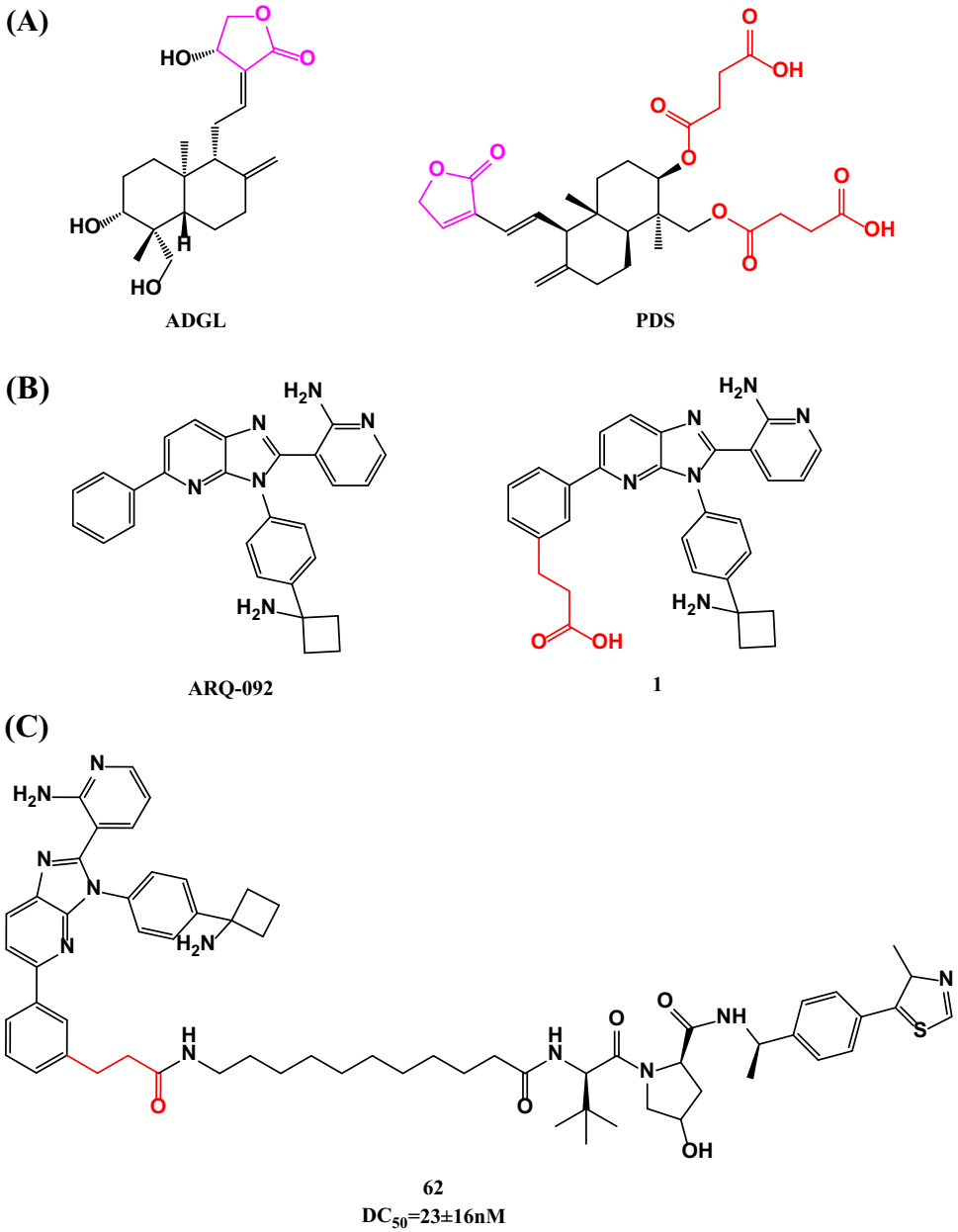

Fig. 1 Chemical structures of covalent inhibitors The chemical structures of ADGL and its derivative PDS.(**A**), The chemical structures of ADQ-092 and its derivative 1(**B**),Chemical structure of ARQ-092-Based AKT PROTAC 62 (**C**)

[19]. Based on this premise, we will employ the PROTAC strategy to synthesize a series of "PDS-PROTACs" utilizing andrographolide as the lead compound, with the aim of improving degradation activity against EGFR.

EGFR is a receptor tyrosine kinase that plays a pivotal role in the regulation of cell proliferation, differentiation, and survival [20]. Its overexpression has been documented in various human cancers, particularly in breast cancer, where it is associated with aggressive tumor behavior and poor clinical prognosis [21]. Aberrant EGFR signaling promotes tumor progression through sustained activation of downstream pathways, including the JAK2/STAT3 axis, contributing to resistance against apoptosis and enhanced metastatic potential. Despite the clinical use of EGFR inhibitors, their therapeutic efficacy remains limited by drug resistance, off-target effects, and insufficient degradation of the receptor protein itself. Therefore, a strategy that not only inhibits but also depletes EGFR could represent a transformative advancement in targeted cancer therapy.

In this study, we designed and synthesized a novel series of PROTAC molecules by conjugating PDS with CRBN ligands, aiming to achieve targeted EGFR degradation. By leveraging the bioactive scaffold of a clinically approved natural product and the event-driven mechanism of PROTACs, our work proposes an innovative approach to address the limitations of traditional EGFR inhibition and explore a new therapeutic avenue for breast cancer treatment.

Results and discussion

Design and synthesis of novel dual PROTACs targeting EGFR

Molecular docking

Andrographolide, known for its significant anti-cancer activities, particularly against breast, lung, and cervical cancers, retains an important pharmacophore—the α-methylene-γ-butyrolactone moiety—in its derivative PDS [20]. Leveraging molecular similarity principles.

PDS was subjected to molecular docking with potential targets of andrographolide, including SRC, BRAF, CASP3, EGFR, and MMP2 [21], to identify optimal binding models. As shown in Table 1 and Fig. 2, the lowest binding energies from the molecular docking of PDS with SRC, BRAF, CASP3, EGFR, and MMP2 were −4.76 kJ/mol, −6.72 kJ/mol, −7.18 kJ/mol, −6.47 kJ/mol, and −4.34 kJ/mol, respectively. CASP3 exhibited the strongest binding affinity with PDS, followed by BRAF. However, considering that CASP3 is an apoptosis-promoting protein [22] and BRAF is not frequently expressed in breast cancer, we selected EGFR as the focus of subsequent research, given that PDS-based PROTACs aim to degrade specific target proteins.

Table 1 The lowest binding energy result for the molecular docking of PDS with SRC, BRAF,CASP3,EGFR and MMP2

Mode	Binding energy(kcal/mol)				
	SRC	BRAF	CASP3	MMP2	EGFR
1	−4.76	−6.72	−7.18	−4.34	−6.47
2	−4.53	−6.42	−6.74	−3.67	−6.12
3	−4.45	−6.38	−5.65	−3.65	−5.62
4	−4.32	−6.34	−5.46	−3.60	−5.51
5	−3.76	−6.20	−5.40	−3.53	−5.44
6	−3.72	−6.13	−5.31	−3.43	−5.26
7	−3.68	−6.12	−5.27	−3.42	−5.23
8	−3.56	−6.05	−4.97	−3.20	−5.05
9	−3.49	−6.05	−4.94	−3.15	−4.99
10	−3.44	−6.02	−4.91	−3.10	−4.84

To gain a deeper understanding of the interaction between the POI ligand and the target protein, we further analyzed the molecular docking results between PDS and EGFR (Fig. 3A, B). It was observed that the structural modifications in PDS preserved its affinity for EGFR, with the calculated optimal binding energy being −6.47 kJ/mol. The docking analysis revealed significant hydrogen bonding interactions between PDS and EGFR residues, including (Lys757), arginine (Arg836), tyrosine (Tyr869), histidine (His870),and glutamic acid (Glu872), with an average bond length of 2.3 Å.Furthermore, non-bonding interactions between PDS and EGFR proteins result in the formation of forces charaterized by electrostatic potential energy and van der Waals forces(Fig. 3C, D). Additionally, the two carboxyl groups in the PDS structure were exposed to the solvent environment(Fig. 3E), suggesting that these sites could be utilized for the synthesis of PDS-PROTACs.These results provide further confirmation that PDS demonstrates a strong binding interaction with EGFR.

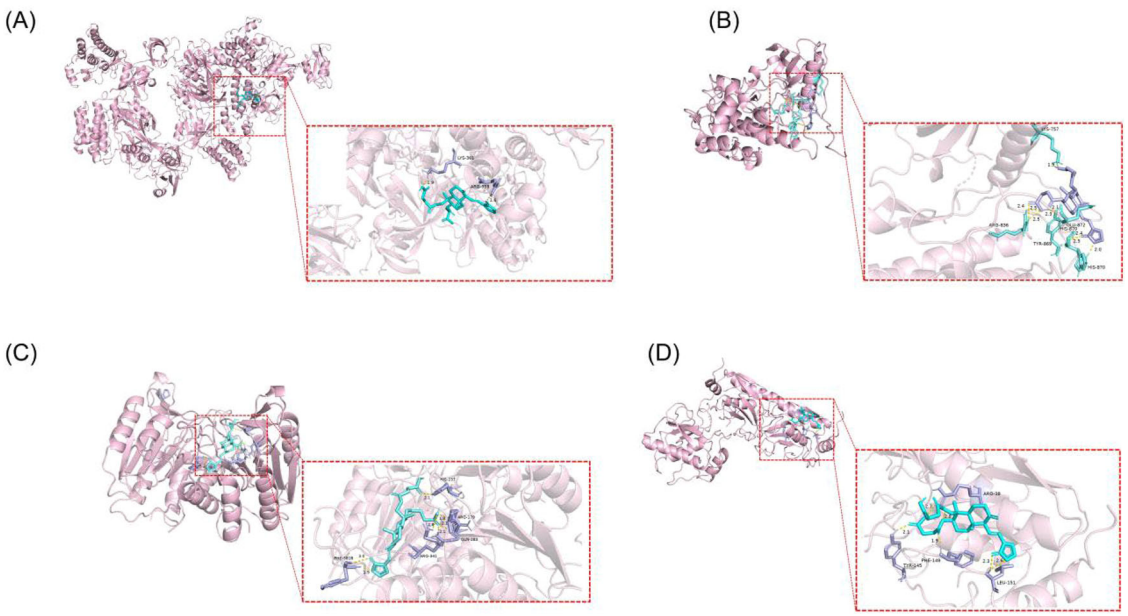

Fig. 2 Molecular docking of PDS with SRC(**A**), BRAF(**B**), CASP3(**C**) and MMP2 (**D**)

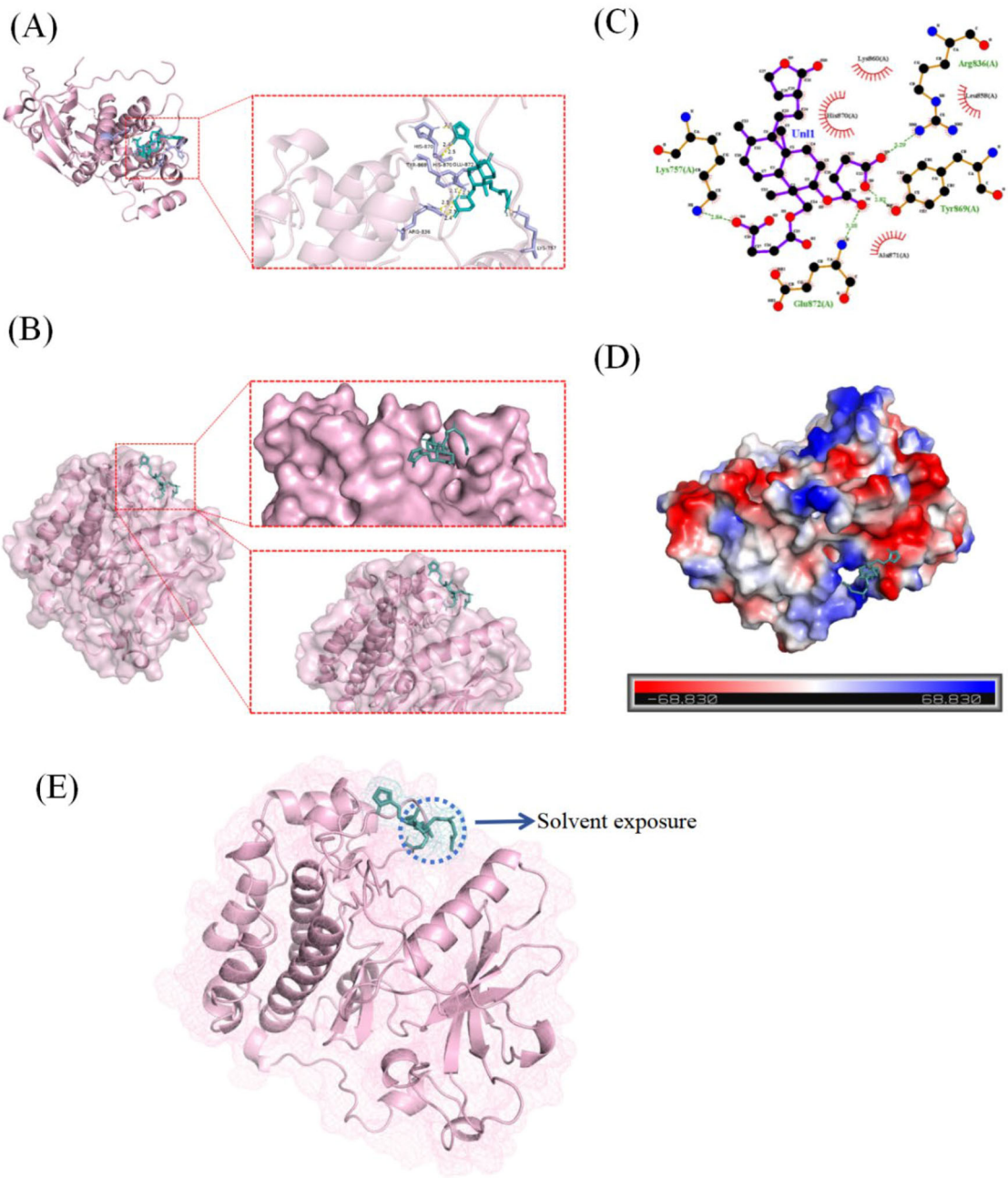

Fig. 3 The predicted binding mode of PDS with EGFR (PDB ID:1I-VO).Three-dimensional structure of PDS-EGFR docking(**A**) PDS and EGFR binding site prediction(**B**),PDS and EGFR binding 2D structural map(**C**),Surface electrostatic forces of PDS and EGFR binding(**D**),The two carboxyl groups of PDS (indicated by the blue circle) is solvent-exposed(**E**)

Chemical synthesis

Amidation is a common coupling reaction in PROTAC synthesis, and the carboxyl groups of PDS were selected as the linker attachment points. Inspired by the successful design of novel dual-PROTACs using Olaparib, Gefitinib, and an E3 ligase ligand conjugated with a star-shaped linker by Li et al. [23], we designed a series of dual-PROTAC molecules based on the structure of PDS. These dual-PROTACs consist of one POI ligand, two linkers, and two E3 ligase ligands (Fig. 4A). The dual-PROTAC molecule specifically recognizes and binds to the target protein via one end of the POI ligand, while the two linkers each bind to the same E3 ubiquitin ligase ligand, forming a "target protein-PROTAC-E3 ligase" quaternary complex. Within this complex, the target protein undergoes simultaneous ubiquitination by two E3 ligases, leading to its recognition and degradation by the proteasome (Fig. 4B).

Currently, available linkers include flexible alkyl chains and polyethylene glycol (PEG) chains, as well as rigid heterocycles,

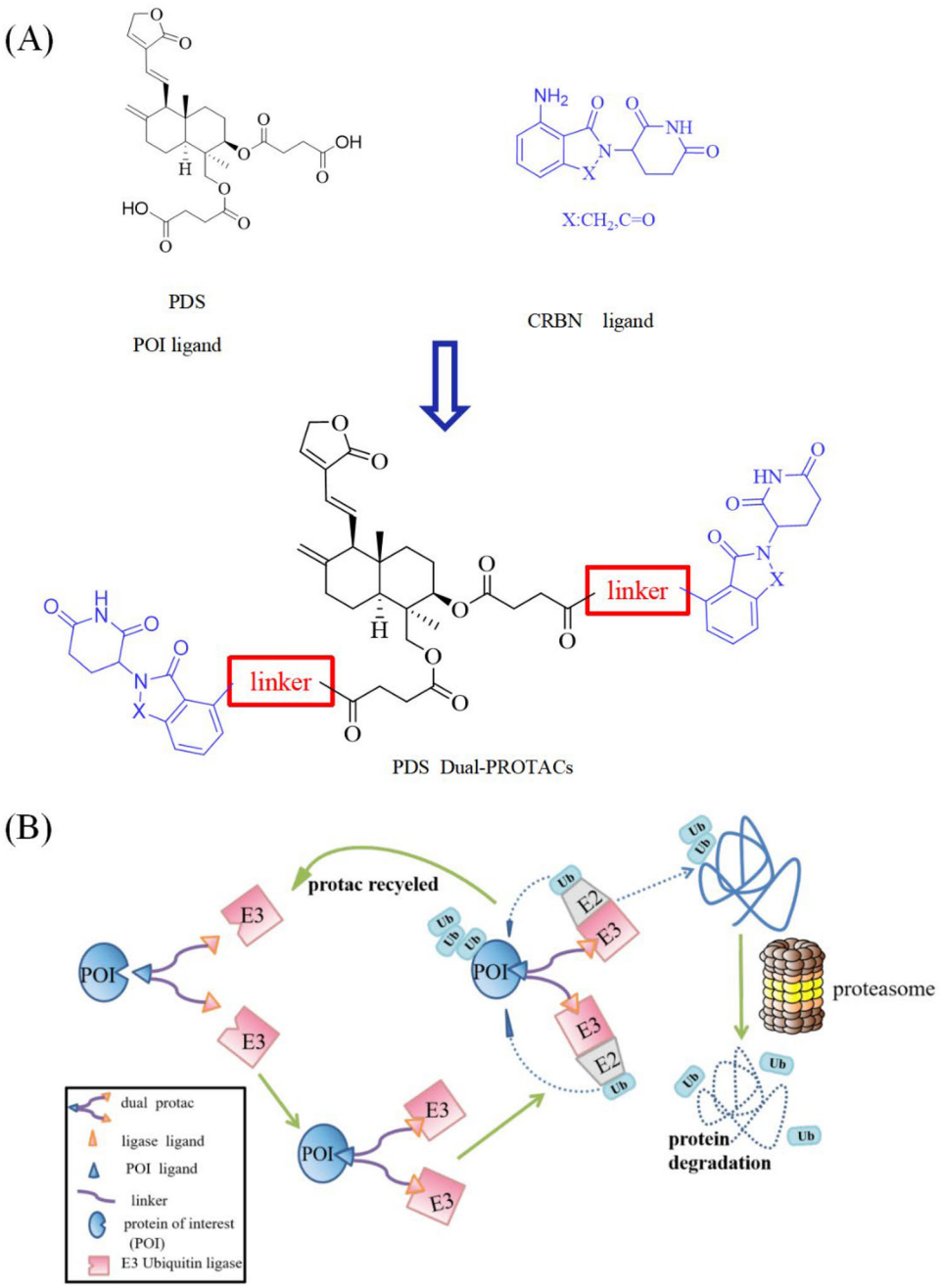

Fig. 4 Design of Dual PROTACS base on PDS (**A**) Design Strategies Based on PDS (**B**) Degradation mechanism of Dual PROTACS

alkyne-containing chains, piperazines, triazoles, and piperidines. The type, length, and polarity of the linker influence the recruitment of the E3 ubiquitin ligase and the formation of the ternary complex, thereby affecting the degradation efficiency and selectivity of PROTACs [24]. Among these, flexible chains are most commonly used due to their conformational flexibility, which enhances the interaction between the PROTAC, POI, and E3 ubiquitin ligase. As of 2023, 44.81% of PROTACs have used alkyl chains and 22.5% have used PEG chains [25]. Based on this data, we selected alkyl and PEG linkers of varying lengths to explore their impact on anti-tumor activity.

The E3 ligase ligands used in PROTACs are mainly derived from VHL and CRBN [26]. Compared to VHL ligands, CRBN ligands exhibit lower molecular weights and better physicochemical and pharmacokinetic properties [27–29]. Hence, our focus was on designing PROTACs using CRBN ligands, specifically pomalidomide and lenalidomide. Additionally, Bricelj et al. demonstrated that PROTACs with a linker introduced at the C-4 position of the phthalimide moiety of CRBN ligands exhibited better stability [30], thus guiding our selection of the C-4 position for linker introduction in this study.

Scheme 1 Synthesis of Compounds DP1-DP9.

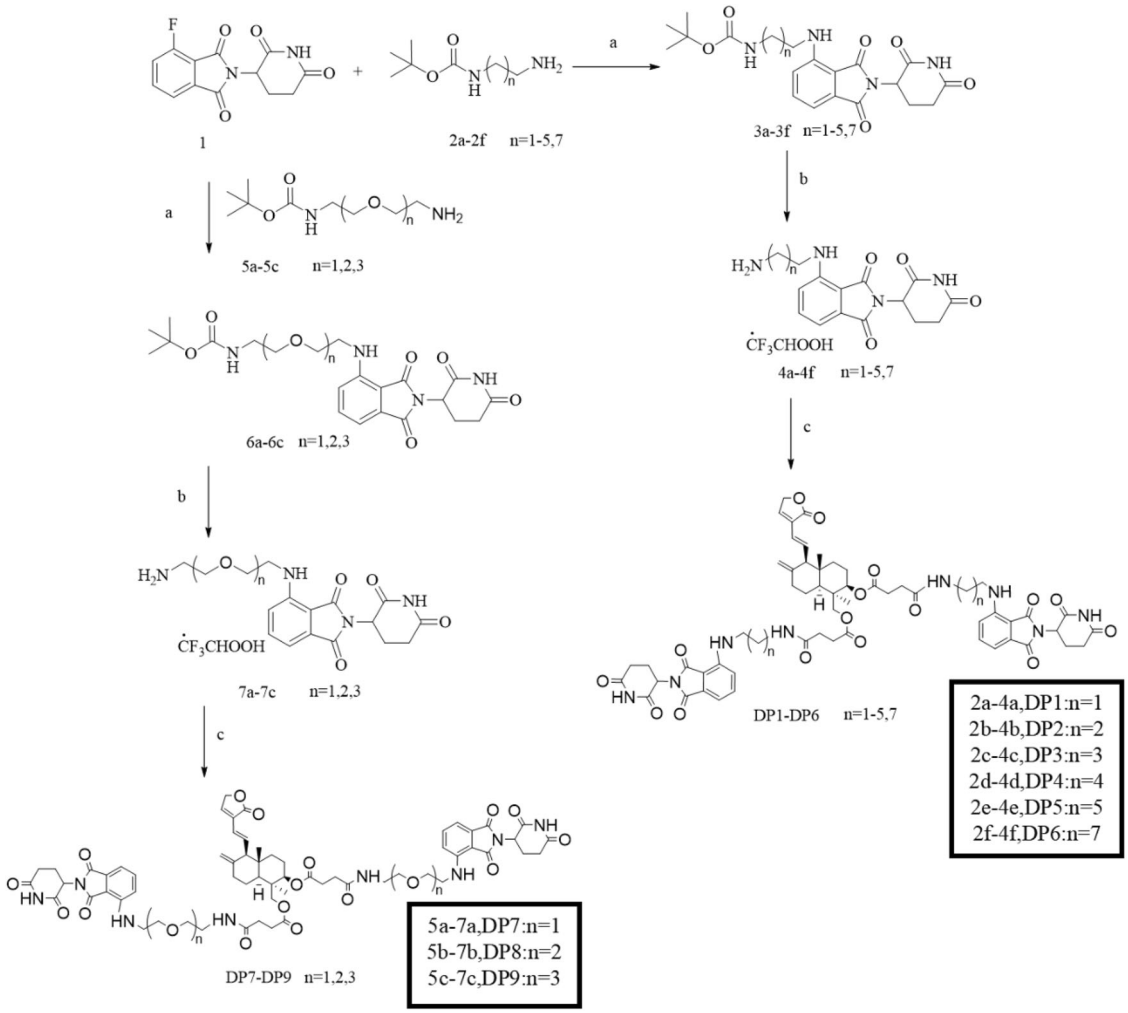

[a]Reagents and conditions: (a) DIPEA, DMF, 90 °C; (b)TFA,DCM/MeOH, rt; (c)PDS,EDCl, HOBt, DIPEA,DMF, rt

Following the proposed design strategy, all compounds were synthesized using standard protocols [31, 32]. The synthesis of compounds **DP_1-DP_9** is shown in Scheme 1. Fluoro-thalidomide was subjected to nucleophilic substitution with alkyl and PEG chains of varying lengths to produce intermediates 3a–3f and 6a–6c. The Boc protective groups were removed under 25% TFA/DCM conditions, and PDS was conjugated with the intermediates via amide condensation reactions to yield the final products **DP_1-DP_9**.

DOPA and 9-((tert-butoxycarbonyl)amino)nonanoic acid underwent an amide formation reaction to produce intermediate 9 under DIPEA/HATU conditions. Subsequently, under acidic conditions (25% CF_3COOH), the Boc protecting group was removed to yield compound 10. Amide formation between EDCl/HoBt/DIPEA and PDS yielded**DL1**(Scheme 2). Purification was subsequently performed using column chromatography and preparative thin-layer chromatography (PTLC). The compounds were structurally characterized using ^{1}H NMR, ^{13}C NMR.

In vitro anti-tumor activity of PDS-PROTACs

To evaluate the efficacy of PDS-based PROTACs in degrading EGFR, two human cancer cell lines overexpressing EGFR were selected, and the biological activities of the synthesized PDS-derived PROTACs were assessed. Tripterine (Celastrol) was used as a positive control [33]. Using the CCK-8 assay, the anti-proliferative effects of PDS and its PROTACs were evaluated against two human cancer cell lines: breast cancer (MCF-7) and non-small cell lung cancer (A549). Various concentrations of PDS, **DP_1-DP_9**, and**DL1** (ranging from 6.125 μM to 400 μM) and different concentrations of Celastrol (ranging from 0.3125 μM to 20 μM) were tested against the cancer

Scheme 2 Synthesis of CompoundsDL1.

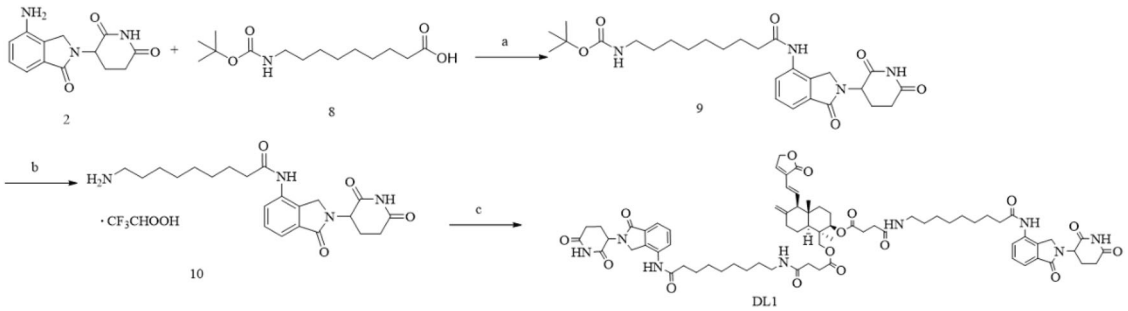

[a]Reagents and conditions: (a) DIPEA, HATU, RT, 24 h; (b)TFA,DCM/MeOH, rt; (c) PDS,EDCl, HOBt,DIPEA,DMF, rt

Table 2 IC_{50} values of compounds PDS,**DP1-DP9,DL1** and Celastrol in A549 and MCF-7

Compounds	IC_{50}(μM)[a]	
	MCF-7	A549
PDS	89.07 ± 6.16	>100
DP1	>100	>100
DP2	>100	>100
DP3	>100	>100
DP4	77.88 ± 9.40	>100
DP5	42.51 ± 2.04	34.17 ± 1.09
DP6	23.60 ± 0.36	26.95 ± 0.22
DP7	>100	>100
DP8	>100	>100
DP9	>100	>100
DL1	68.20 ± 14.80	>100
Celastrol	0.87 ± 0.05	0.23 ± 0.01

[a]The blank group was cultured with DMSO treatment.

Data are from three independent experiments and are presented as mean ± SD.

cells for 48 h. The IC_{50} values of each compound were calculated using SPSS 22.0 software. As shown **in** Table 2, compound **DP6** exhibited the most significant anti-tumor activity across all two cancer cell lines. In MCF-7 cells, **DP6** demonstrated the strongest anti-tumor activity with an IC50 of 23.60 ± 0.36 μM, a 3.8-fold improvement over its precursor, PDS (IC50 = 89.07 ± 6.16 μM). Furthermore, **DP6** showed notable anti-tumor effects against A549 (IC50 = 26.95 ± 0.22 μM) cells, displaying 3.7-fold increase in potency compared to PDS in these cell lines, respectively. Among the synthesized dual PROTACs, DP6 exhibited the most potent antiproliferative activity against MCF-7 cells, with an IC_{50} value of XX μM, and was therefore selected for further mechanistic investigation. Given its superior efficacy, we inferred that the linker length used in DP6 represented an optimal configuration for ternary complex formation. To evaluate whether the dual-ligand design was essential for activity enhancement, we synthesized a monovalent control compound, SP6-1 and SP6-2 (Scheme S1), which retained the same linker and POI ligand as DP6 but incorporated only a single CRBN ligand. As shown in the Supporting Information (Table S1), SP6 exhibited negligible antiproliferative activity, with an IC_{50} exceeding 100 μM, in contrast to the robust efficacy of DP6. This result supports the hypothesis that the dual E3 ligase ligand architecture is critical for maximizing EGFR degradation and anti-tumor potency.

The cell viability assays revealed that PDS was inactive against A549 cells and exhibited only weak antiproliferative effects against MCF-7 cells. The length of the linker was shown to significantly impact the formation of the POI-PROTAC-E3 ternary complex, which is crucial for determining its biological activity [34]. Specifically, alkyl linkers were used to conjugate PDS with pomalidomide ligands, producing PROTACs containing 2–8 methylene units (**DP_1-DP6**). As shown in Fig. 5, there was a clear correlation between linker length and PROTAC activity. Novel compounds DP1-DP3, which had linkers consisting of only 2–4 methylene units, had IC_{50} values greater than 100 μM in all two cancer cell lines, suggesting that shorter linkers may lead to steric hindrance, disrupting the formation of the ternary complex and reducing antiproliferative activity [35]. Increasing the linker length by one methylene unit in DP4 resulted in a slight improvement in anti-proliferative activity in MCF-7 cells (IC_{50} = 77.88 ± 9.40 μM). Further increasing the linker length in DP5 led to a significant improvement in anti-tumor activity, with IC_{50} values of 42.51 ± 2.04 μM in MCF-7 cells and 34.17 ± 1.09 μM in A549 cells. When the linker was extended to 8 methylene units, the resulting PROTAC (**DP6**) exhibited the most potent anti-tumor activity in all two cell lines, showing a 3.8-fold and 2.9-fold

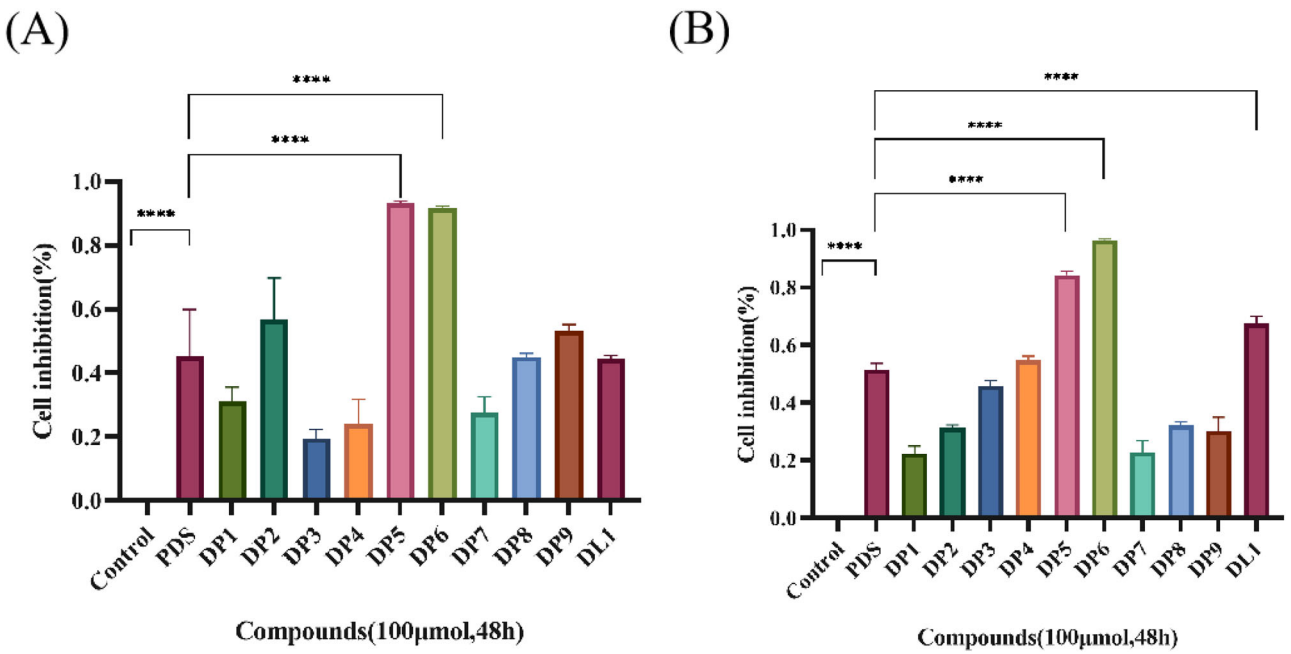

Fig. 5 Effect of different PROTACs of PDS on the inhibition of two tumor cells, (**A**) A549 and (**B**) MCF-7 cells. The blank group was cultured with DMSO treatment. The bar graphs are presented as mean ± SD.*Statistical analysis was performed by one-way ANOVA. n = 3**** = P < 0.0001 vs control group*

improvement in MCF-7 and A549 cells, respectively, compared to its precursor PDS (Fig. 5A, B). The significant increase in potency indicated a notable shift in the mechanism of action of the new compound. However, compared to alkyl linkers, compounds with PEG linkers did not demonstrate significant anti-tumor activity (IC50 > 100 μM). **DP6** and**DL1**, both of which contain an 8-methylene alkyl linker, differed only in the structure of their E3 ligase ligand, with **DP6** conjugating pomalidomide and**DL1** conjugating lenalidomide. **DP6** exhibited more potent anti-proliferative activity in MCF-7 cells, while **DL1** showed no significant activity in A549 cells and a 2.9-fold reduction in potency in MCF-7 cells. Zhao et al. previously reported that CT-4, a PROTAC designed to selectively degrade HDAC8, exhibited significant anti-migratory and anti-proliferative activity in MDA-MB-231 cells, with the PROTAC linker consisting of 8 methylene units [36]. This suggests that pomalidomide may be a more suitable E3 ligase ligand than lenalidomide, and the use of an 8-methylene alkyl linker may enhance anti-tumor activity.

DP6 degrades EGFR proteins in MCF-7 breast cancer cells via the ubiquitin-proteasome pathway and inhibits the JAK2-STAT3 downstream signaling pathway

To explore the potential therapeutic targets of **DP6** in breast cancer, we conducted Western blot analysis. MCF-7 cells were treated with varying concentrations of **DP6** (10 μM, 20 μM, 30 μM, and 40 μM) for 48 h, and EGFR degradation was assessed. The results were compared with the degradation effects of 40 μM PDS. The study demonstrated that **DP6** induced a concentration-dependent degradation of EGFR, with degradation increasing progressively with concentration and reaching near-complete degradation at 30 μM. Notably, 10 μM of **DP6** exhibited degradation effects comparable to 40 μM of PDS, while 40 μM of **DP6** completely degraded EGFR, representing the most potent degradation activity (Fig. 6A).

To further investigate whether **DP6** induces EGFR degradation through the ubiquitin-proteasome system,we assessed the reliance of **DP6**-induced EGFR degradation on proteasome activity using the proteasome inhibitor MG132, which is widely applied to inhibit proteasome activity. Inhibition of the proteasome by MG132 significantly reduced **DP6**-induced EGFR degradation (Fig. 6B). These results inducated our hypothesis that PDS-based PROTACs can promote the proteasome-dependent degradation of EGFR.Although the formation and demonstration of ternary complexes is necessary for a more direct demonstration of the degradation of EGFR by **DP6**, our intention at this stage is only to demonstrate the degradation efficiency of EGFR by **DP6**. In subsequent studies, we will explore the formation of ternary complexes even further.

EGFR participates in signal transduction and transcriptional activation through the classical JAK/STAT3 signaling pathway [37]. Its overexpression activates downstream pathways, promoting the expression of anti-

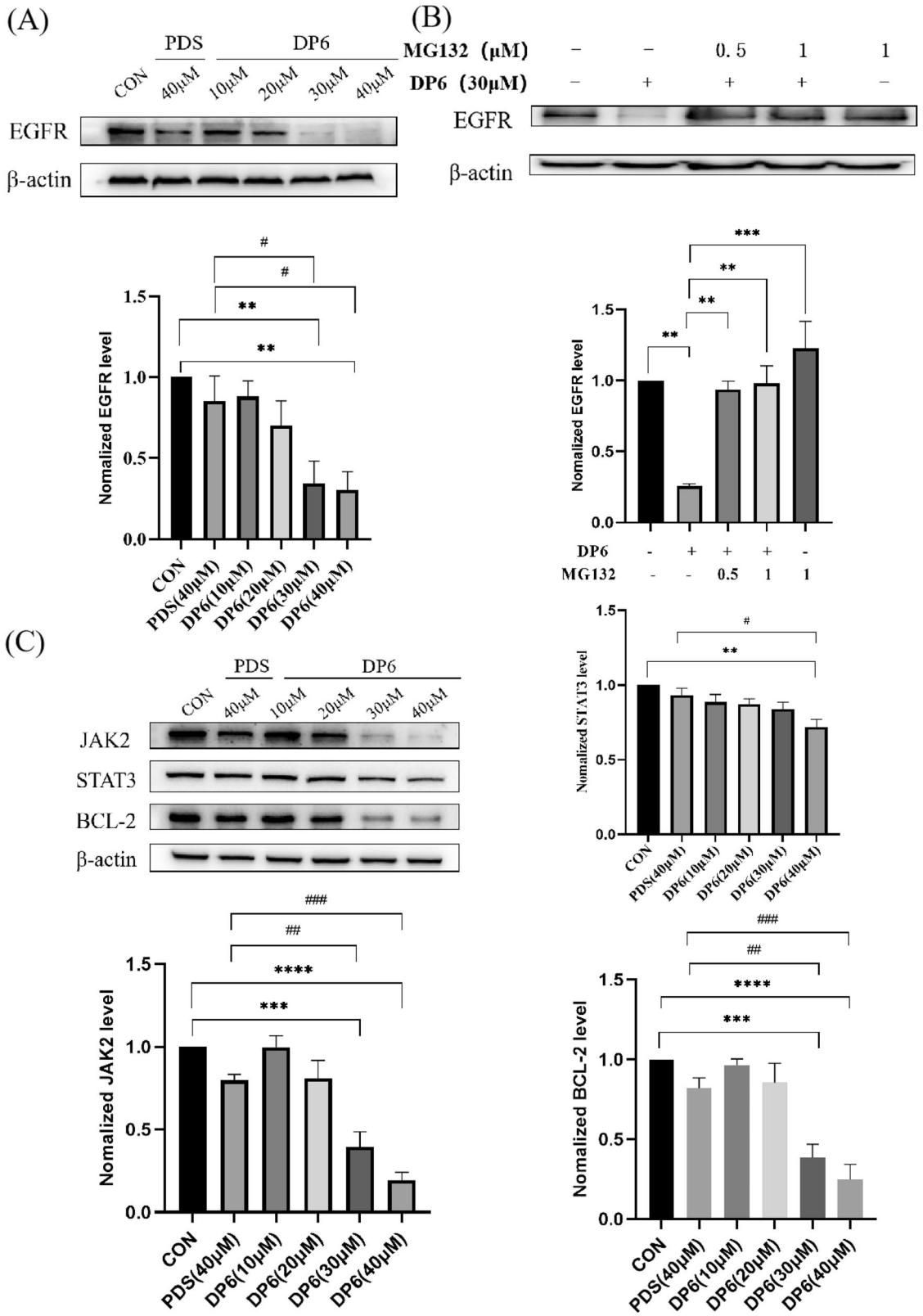
(A)
PDS
DP6
CON
40μM
10μM
20μM
30μM
40μM
EGFR
β-actin
Nomalized EGFR level
CON
PDS(40μM)
DP6(10μM)
DP6(20μM)
DP6(30μM)
DP6(40μM)
(B)
MG132 (μM) – – 0.5 1 1
DP6 (30μM) – + + + –
EGFR
β-actin
Nomalized EGFR level
DP6 - + + + -
MG132 - - 0.5 1 1
(C)
PDS
DP6
JAK2
STAT3
BCL-2
β-actin
Nomalized JAK2 level
Nomalized STAT3 level
Nomalized BCL-2 level

◀ **Fig. 6** **DP6** degrades EGFR proteins in MCF-7 breast cancer cells via the ubiquitin-proteasome pathway and inhibits the JAK2-STAT3 downstream signaling pathway. (**A**) Western blot analyses of EGFR with lysates generated from MCF-7 cells treated with PDS (40 μM) and **DP6** (10, 20, 30 and 40 μM); (**B**) MCF-7 cells were pre-treated with MG132 for 3 h, then with DMSO or **DP6** for 48 h; Western blot analysis was used to estimate and the band intensity was calculated by ImageJ software. The bar graphs are presented as mean ± SD. Statistical analysis was performed by one-way ANOVA. n = 3, ** $p < 0.005$, *** $p < 0.001$ compared with the 30 μM **DP6** group.(**C**) The effect of PDS (40 μM) and **DP6** on JAK2, STAT3 and BCL-2 levels.The blank group was cultured with DMSO treatment.Western blot analysis was used to estimate and the band intensity was calculated by ImageJ software. The bar graphs are presented as mean ± SD. Statistical analysis was performed by one-way ANOVA. n = 3, #= $P < 0.05$;## = $P < 0.01$;### = $P < 0.001$ vs PDS group, * = $P < 0.05$;** = $P < 0.01$;*** = $P < 0.001$;**** = $P < 0.0001$ vs control group

apoptotic genes such as BCL-2, which supports cancer cell proliferation. Therefore, we further investigated the impact of EGFR degradation on the JAK/STAT3 signaling pathway and the expression of anti-apoptotic protein BCL-2. Western blot analysis revealed that increasing concentrations of **DP6** led to a significant decrease in JAK2, STAT3, and BCL-2 expression levels (Fig. 6C). These findings suggest that **DP6** promotes breast cancer cell apoptosis and inhibits cancer progression by degrading EGFR, suppressing the JAK2-STAT3 signaling pathway, and reducing BCL-2 expression.

Preliminary in silico ADME evaluation and developability assessment

To assess the drug-likeness and developability of the designed PROTAC molecules, we performed an in silico ADME evaluation of representative compounds (DP1–DP7, DL1, and SP6) using the SwissADME platform [38]. As expected for PROTACs, all compounds exhibited high molecular weights (1129–1297 Da), a large number of rotatable bonds (25–37), and multiple violations of Lipinski, Ghose, and Veber rules, consistent with their size and complexity. Despite these unfavorable drug-likeness parameters, the compounds showed no PAINS or structural toxicity alerts, indicating clean molecular frameworks. Notably, the lead compound DP6 demonstrated the most potent anti-proliferative activity and also displayed a favorable safety profile, with no toxic substructures, moderate hydrogen-bonding potential, and a bioavailability score of 0.17.

Further analysis revealed that the predicted water solubility of DP6 was low (logS < –5), which is consistent with the poor aqueous solubility commonly observed in high-MW PROTAC molecules and may pose a challenge for oral delivery. Although no experimental metabolic stability studies were conducted in this study, the structural analysis showed no metabolic liability alerts, and the presence of multiple amide bonds suggests possible enzymatic resistance. These findings point to the need for further pharmacokinetic characterization and formulation optimization, but also support the potential of DP6 as a tractable lead compound with a clean toxicity profile.

Due to the excessive size and flexibility of DP8 and DP9, SwissADME was unable to process these molecules for in silico evaluation, and they were thus excluded from this assessment. Future work will employ alternative prediction models or experimental validation to explore the pharmacokinetic properties of these higher-molecular-weight candidates.

Conclusion

In conclusion, we successfully designed and synthesized a novel series of dual PROTAC molecules by conjugating the natural product-derived ligand PDS with two CRBN ligands via rationally optimized linkers. This dual-ligand architecture was intended to improve ternary complex formation efficiency and promote more robust degradation of EGFR. Among the synthesized compounds, DP6 demonstrated superior anti-proliferative activity in EGFR-overexpressing breast cancer cells and effectively induced EGFR degradation via the ubiquitin–proteasome pathway. Mechanistic studies further revealed that EGFR depletion by DP6 suppressed the downstream JAK2-STAT3 signaling cascade and reduced BCL-2 expression, ultimately promoting cancer cell apoptosis.

These findings validate the feasibility of converting structurally active natural product derivatives into functional PROTACs and highlight the dual PROTAC strategy as a promising approach to enhance degradation efficiency beyond conventional single-ligand designs. Moving forward, further investigations will be conducted to evaluate the in vivo pharmacokinetic profile, anti-tumor efficacy, and safety of DP6 in animal models. Moreover, structural optimization of linkers and ligands may further improve drug-like properties and target selectivity. Given the versatility of this design strategy, the dual PROTAC approach may also be extended to other oncogenic proteins beyond EGFR, offering a new direction for the development of natural product-based targeted therapies.

Method

Cell culture

MCF-7 (human breast cancer cells) and A549 (human non-small cell lung cancer cells) were obtained from Wuhan Procell Life Technology Co., Ltd. and cultured as required. RPMI-1640 culture medium and fetal bovine serum (FBS) were purchased from Gibco (USA), and a penicillin-

streptomycin solution was obtained from Beijing Solarbio Life Sciences Co., Ltd. Phosphate-buffered saline (PBS) was purchased from Wuhan Procell Life Technology Co., Ltd., and CCK-8 assay kits were acquired from Shanghai Beyotime Biotechnology Co., Ltd.

Cell viability assay

MCF-7 and Hela cells in the logarithmic growth phase were diluted with 1640 medium containing 10% FBS. After counting, the cells were seeded in 96-well plates at a density of 10^5 cells/ml and incubated at 37 °C with 5% CO_2 for 24 h.

Next, the medium was replaced with different concentrations of the PROTAC compounds dissolved in DMSO (ranging from 6.125 μM to 400 μM), with triplicate wells for each sample. Additionally, Celastrol at various concentrations (ranging from 0.3125 μM to 20 μM) dissolved in DMSO was used as a positive control. After a 48-h incubation period, CCK-8 reagent was added to each well, followed by a 0.5-h incubation, and the absorbance at 450 nm was measured using a microplate reader. The inhibition rate of cell growth was calculated using the following formula: (OD value of control well-OD value of drug-treated well)/(OD value of control well-OD value of blank well). The IC50 values were calculated using SPSS 22.0 software.

Western blot analysis of EGFR, JAK2, STAT3, and BCL-2 expression levels

After 48 h of incubation with the compounds at 37 °C and 5% CO_2, MCF-7 cells were harvested by centrifugation and lysed in a buffer containing 0.5% glycerol, 1% Triton X-100, 50 mM Tris-HCl (pH 7.4), 150 mM NaCl, 20 mM NaF, 2 mM Na_3VO_4, 0.1 mM leupeptin, and 2 mM PMSF. Total protein was extracted and subjected to Western blotting. Proteins were separated by SDS-PAGE at 100 V for 90 min and transferred to PVDF membranes (Merck Millipore Ltd., USA). The membranes were blocked with a blocking solution (5% non-fat milk, 2% Tween-20, 1× PBS) for 1 h, washed with TBST buffer, and incubated with primary antibodies overnight at 4 °C. The following primary antibodies were used: anti-EGFR (1:5000 dilution), anti-JAK2 (1:4000), anti-BCL-2 (1:2000), anti-STAT3 (1:10000), and anti-β-actin (1:10000). Secondary antibodies conjugated with horseradish peroxidase (HRP) were used for detection. The protein bands were visualized using an ECL chemiluminescence detection kit (Biosharp, China), and band intensity was quantified using ImageJ software.

Molecular docking

The structures of SRC, BRAF, CASP3, EGFR, and MMP2 proteins were downloaded from the Protein Data Bank (PDB) database and preprocessed using PyMOL software to remove water molecules and non-protein components. The processed structures were saved in PDB format. Next, the structures were imported into AutoDockTools for preparation, where hydrogen atoms were added, Gasteiger charges were calculated, and AD4 atom types were assigned. The prepared protein structures were saved in .pdbqt format.

For ligand preparation, ChemDraw 3D was used to generate the PDB structure of the ligand, which was then converted to .pdbqt format using AutoDockTools. Molecular docking was performed, and the best docking conformations were selected based on binding energies. The interactions between the ligand and the target proteins were analyzed using PyMOL.

EGFR degradation pathways evaluation

Cells were seeded at a density of 2×10^5/ml cells per well in 6-well plates and incubated in 37 °C, 5% CO_2 cell incubator for 24 h. Preceding the addition of **DP6** (30 μM) for a 48 h incubation period,pretreatment with MG132 (0.5 μM and 1.0 μM) was carried out for 3 h. Subsequently,total protein was collected and subjected to analysis through immunoblotting.

Chemistry section

Unless otherwise stated, all chemical reactions were performed under dry conditions in glassware equipped with magnetic stirring. All reagents and solvents were obtained commercially and used without further purification. Reaction progress was monitored by thin-layer chromatography (TLC), and the mobile phases consisted of dichloromethane/methanol or petroleum ether/ethyl acetate systems. TLC spots were visualized by iodine staining or under UV light at 254 nm or 365 nm. TLC plates were dipped into a 10% H_2SO_4 ethanol solution and heated on a hot plate. Crude products were purified using preparative thin-layer chromatography (PTLC) and silica gel column chromatography (200–300 mesh). ^1H NMR and ^{13}C NMR spectra were recorded on a Bruker III-500 spectrometer at room temperature, using tetramethylsilane (TMS) as the internal standard. Chemical shifts are expressed in parts per million (δ), and coupling constants are reported in Hertz (Hz). Before use, reagents such as ethyl acetate, dichloromethane, methanol, petroleum ether, and N,N-dimethylformamide (DMF) were dehydrated with molecular sieves. Finally, HRMS was used to identify the final Product DP_1-DP_9, and DL_1.

Synthesis of DP1-DP9 PROTACs

Synthesis of tert-butyl (2-((2-(2,6-dioxopiperidin-3-yl)-1,3-dioxoisoindolin-4-yl)amino)ethyl) carbamate (3a)

To a solution of N-Boc-1,2-diaminoethane (1.2 eq, 4.90 mmol) and fluorothalidomide (1.0 eq, 4.08 mmol)

in dry DMF (2.0 mL), DIPEA (2.0 eq, 8.16 mmol) was added under stirring, and the mixture was refluxed at 90 °C for approximately 12 h, with reaction progress monitored by TLC. Upon completion, the reaction was quenched with ice water, and the mixture was extracted with ethyl acetate. The organic layers were combined, washed with saturated $NaHCO_3$ and brine, dried over anhydrous Na_2SO_4, filtered, and concentrated under reduced pressure. The crude product was purified by silica gel column chromatography (petroleum ether: ethyl acetate = 1:1), yielding a green fluorescent powder (intermediate 3a) with a yield of 40.7%0.^{1}H NMR (500 MHz, DMSO-d6): δ 11.10 (s, 1H), 7.57 (t, J = 7.8 Hz, 1H), 7.14 (d, J = 8.6 Hz, 1H), 7.03 (s, 1H), 7.02 (s, 1H), 6.71 (s, 1H), 5.05 (dd, J = 12.8, 5.4 Hz, 1H), 3.37 (d, J = 6.5 Hz, 2H), 3.14 – 3.10 (m, 2H), 2.88 (d, J = 2.2 Hz, 1H), 2.58 (dd, J = 17.3, 3.0 Hz, 1H), 2.01 (d, J = 5.6 Hz, 1H), 1.36 (s, 9H), 1.23 (s, 1H); ^{13}C NMR (126 MHz, DMSO-d6): δ 172.79, 170.03, 168.70, 167.30, 155.89, 146.41, 136.17, 132.21, 117.07, 110.49, 109.24, 77.79, 54.89, 48.52, 41.59, 30.97, 28.19, 22.17.

Synthesis of tert-butyl (3-((2-(2,6-dioxopiperidin-3-yl)-1,3-dioxoisoindolin-4- yl)amino) pro-pyl) carbamate (3b)

The synthesis of 3b followed the same procedure as 3a, replacing N-Boc-1,2-diaminoethane with N-Boc-1,3-diaminopropane. A green fluorescent powder was obtained, with a yield of 53.4%.^{1}H NMR (500 MHz, $CDCl_3$): δ 8.39 (s, 1H), 7.53 – 7.43 (m, 1H), 7.08 (d, J = 7.1 Hz, 1H), 6.88 (d, J = 8.5 Hz, 1H), 6.31 (d, J = 6.1 Hz, 1H), 4.91 (dd, J = 12.3, 5.3 Hz, 1H), 4.72 (t, J = 6.1 Hz, 1H), 3.32 (q, J = 6.6 Hz, 2H), 3.24 (d, J = 6.5 Hz, 2H), 2.90 – 2.85 (m, 1H), 2.83 – 2.71 (m, 2H), 2.15 – 2.08 (m, 1H), 1.84 (q, J = 6.8 Hz, 2H), 1.44 (s, 9H); ^{13}C NMR (126 MHz, $CDCl_3$): δ 171.33, 169.56, 168.57, 167.73, 156.25, 146.89, 136.30, 132.63, 116.69, 111.72, 110.24, 79.62, 49.00, 40.14, 38.16, 31.54, 29.96, 28.52, 22.90.

Synthesis of tert-butyl (4-((2-(2,6-dioxopiperidin-3-yl)-1,3-dioxoisoindolin-4-yl)amino)butl) carbamate (3c)

The synthesis of 3c followed the same procedure as 3a, replacing N-Boc-1,2-diaminoethane with N-Boc-1,4-diaminobutane. A green fluorescent powder was obtained, with a yield of 49.1%.^{1}H NMR (500 MHz, $CDCl_3$): δ 8.37 (s, 1H), 7.48 (t, J = 7.9 Hz, 1H), 7.08 (d, J = 7.1 Hz, 1H), 6.86 (d, J = 8.5 Hz, 1H), 6.22 (t, J = 5.6 Hz, 1H), 4.91 (dd, J = 12.2, 5.3 Hz, 1H), 4.59 (t, J = 6.4 Hz, 1H), 3.25 (q, J = 6.6 Hz, 2H), 3.12 (q, J = 9.0, 7.9 Hz, 2H), 2.91 – 2.83 (m, 1H), 2.81 – 2.70 (m, 2H), 2.11 (dd, J = 11.3, 5.4 Hz, 1H), 1.75 (s, 2H), 1.67 (t, J = 7.5 Hz, 2H), 1.52 (d, J = 7.6 Hz, 2H), 1.43 (s, 9H); ^{13}C NMR (126 MHz, $CDCl_3$): δ 171.30, 169.64, 168.59, 167.76, 156.14, 147.06, 136.26, 132.61, 116.76, 111.57, 110.03, 79.32, 48.99, 42.66, 40.49, 31.53, 29.97, 29.81, 29.04, 28.54, 24.27, 22.92.

Synthesis of tert-butyl (5-((2-(2,6-dioxopiperidin-3-yl)-1,3-dioxoisoindolin-4- yl)amino) pen-tyl) carbamate (3d)

The synthesis of 3 d followed the same procedure as 3a, replacing N-Boc-1,2-diaminoethane with N-Boc-1,5-diaminopentane. A green fluorescent powder was obtained, with a yield of 46.8%.^{1}H NMR (500 MHz, $CDCl_3$): δ 8.37 (s, 1H), 7.48 (t, J = 7.9 Hz, 1H), 7.08 (d, J = 7.0 Hz, 1H), 6.86 (d, J = 8.5 Hz, 1H), 6.22 (t, J = 5.6 Hz, 1H), 4.91 (dd, J = 12.2, 5.3 Hz, 1H), 4.59 (t, J = 6.4 Hz, 1H), 3.25 (q, J = 6.6 Hz, 2H), 3.12 (q, J = 9.0, 7.9 Hz, 2H), 2.91 – 2.83 (m, 1H), 2.81 – 2.70 (m, 2H), 2.11 (dd, J = 11.3, 5.4 Hz, 1H), 1.75 (s, 2H), 1.67 – 1.63 (m, 2H), 1.52 (q, J = 7.3 Hz, 2H), 1.43 (s, 9H);^{13}C NMR (126 MHz, $CDCl_3$): δ 171.30, 169.64, 168.59, 167.76, 156.14, 147.06, 136.26, 132.61, 116.76, 111.57, 110.03, 79.32, 48.99, 42.66, 40.49, 31.53, 29.97, 29.81, 29.04, 28.54, 24.27, 22.92.

Synthesis of tert-butyl (6-((2-(2,6-dioxopiperidin-3-yl)-1,3-dioxoisoindolin-4- yl)amino) hex-yl)carbamate (3e)

The synthesis of 3e followed the same procedure as 3a, replacing N-Boc-1,2-diaminoethane with N-Boc-1,6-diaminohexane. A green fluorescent powder was obtained, with a yield of 40.5%.^{1}H NMR (500 MHz, $CDCl_3$): δ 8.35 (s, 1H), 7.48 (dd, J = 8.6, 7.1 Hz, 1H), 7.07 (d, J = 7.1 Hz, 1H), 6.86 (d, J = 8.5 Hz, 1H), 6.22 (t, J = 5.6 Hz, 1H), 4.91 (dd, J = 12.3, 5.4 Hz, 1H), 3.28 – 3.22 (m, 2H), 3.10 (d, J = 7.6 Hz, 2H), 2.91 – 2.85 (m, 1H), 2.80 – 2.68 (m, 2H), 2.15 – 2.08 (m, 1H), 1.77 – 1.72 (m, 1H), 1.65 (q, J = 7.3 Hz, 2H), 1.50 – 1.46 (m, 2H), 1.43 (s, 9H), 1.37 (dd, J = 9.0, 5.2 Hz, 2H), 1.24 (s, 1H); ^{13}C NMR (126 MHz, $CDCl_3$): δ 171.28, 169.64, 168.57, 167.76, 155.32, 147.10, 136.25, 132.61, 116.76, 111.53, 109.98, 81.09, 48.98, 43.50, 42.67, 31.53, 30.12, 29.27, 28.55, 26.74, 26.59, 22.92.

Synthesis of tert-butyl (8-((2-(2,6-dioxopiperidin-3-yl)-1,3-dioxoisoindolin-4- yl)amino) oct-yl)carbamate (3f)

The synthesis of 3 f followed the same procedure as 3a, replacing N-Boc-1,2-diaminoethane with N-Boc-1,8-diaminooctane. A green fluorescent powder was obtained with a yield of 39.4%.^{1}H NMR (500 MHz, $CDCl_3$) δ 8.29 (s, 1H), 7.48 (dd, J = 8.5, 7.1 Hz, 1H), 7.08 (d, J = 7.0 Hz, 1H), 6.87 (d, J = 8.5 Hz, 1H), 6.23 (t, J = 5.5 Hz, 1H), 4.91 (dd, J = 12.3, 5.2 Hz, 1H), 4.54 (s, 1H), 3.25 (q, J = 6.5 Hz, 2H), 3.10 (q, J = 6.7 Hz, 2H), 2.91 – 2.84 (m, 1H), 2.81 – 2.71 (m, 2H), 2.12 (m, J = 9.9, 5.1, 2.4 Hz, 1H), 1.67 – 1.62 (m, 2H), 1.43 (s, 9H), 1.31 (d, J = 4.7 Hz, 7H), 1.25 (s,

3H).[13]C NMR (126 MHz, $CDCl_3$) δ 171.21, 169.65, 168.53, 167.78, 156.14, 147.15, 136.24, 132.63, 116.78, 111.49, 109.97, 79.21, 48.99, 42.74, 40.72, 32.05, 31.55, 30.15, 29.83, 29.29, 29.26, 28.56, 26.94, 26.80, 22.95, 14.25.

Synthesis of tert-butyl (2-(2-((2-(2,6-dioxopiperidin-3-yl)-1,3-dioxoisoindolin-4- yl)amino) e-thoxy)ethyl)carbamate (6a)

The synthesis of 6a followed the same procedure as 3a, replacing N-Boc-1,2-diaminoethane with tert-butyl [2-(2-aminoethoxy)ethyl]carbamate. A green fluorescent powder was obtained with a yield of 33.4%.[1]H NMR (500 MHz, $CDCl_3$) δ 8.38 (s, 1H), 7.49 (dd, J = 8.6, 7.1 Hz, 1H), 7.10 (d, J = 7.0 Hz, 1H), 6.91 (d, J = 8.5 Hz, 1H), 6.50 (s, 1H), 5.01 (s, 1H), 4.92 (dd, J = 12.1, 5.3 Hz, 1H), 3.68 (t, J = 5.3 Hz, 2H), 3.55 (t, J = 5.2 Hz, 2H), 3.45 (t, J = 5.3 Hz, 2H), 3.32 (q, J = 5.4 Hz, 2H), 2.93 – 2.83 (m, 1H), 2.82 – 2.59 (m, 2H), 2.11 (ddd, J = 13.2, 6.1, 3.7 Hz, 1H), 1.76 (s, 1H), 1.41 (s, 9H).[13]C NMR (126 MHz, $CDCl_3$) δ 171.29, 169.52, 168.54, 167.72, 156.12, 146.96, 136.23, 132.59, 116.92, 111.91, 110.46, 79.40, 70.39, 69.37, 49.01, 42.35, 40.50, 31.55, 28.50, 22.86.

Synthesis of tert-butyl (2-(2-(2-((2-(2,6-dioxopiperidin-3-yl)-1,3-dioxoisoindolin-4- yl) ami-no)ethoxy)ethoxy)ethyl) carbamate (6b)

The synthesis of 6b followed the same procedure as 3a, replacing N-Boc-1,2-diaminoethane with tert-butyl [2-(2-(2-aminoethoxy)ethoxy)ethyl]carbamate. A green fluorescent powder was obtained with a yield of 29.8%.[1]H NMR (500 MHz, $CDCl_3$) δ 8.40 (s, 1H), 7.49 (dd, J = 8.6, 7.1 Hz, 1H), 7.10 (d, J = 7.1 Hz, 1H), 6.91 (d, J = 8.5 Hz, 1H), 6.50 (t, J = 5.7 Hz, 1H), 5.01 (t, J = 5.6 Hz, 1H), 4.92 (dd, J = 12.2, 5.3 Hz, 1H), 3.68 (t, J = 5.3 Hz, 2H), 3.55 (t, J = 5.2 Hz, 2H), 3.45 (q, J = 5.0 Hz, 2H), 3.32 (q, J = 5.5 Hz, 2H), 2.90 – 2.78 (m, 2H), 2.77 – 2.70 (m, 1H), 2.14 – 2.08 (m, 1H), 1.77 (s, 1H), 1.41 (s, 9H), 1.39 – 0.97 (m, 2H), 0.94 – 0.77 (m, 1H). [13]C NMR (126 MHz, $CDCl_3$) δ 171.30, 169.53, 168.55, 167.72, 156.13, 146.97, 136.23, 132.61, 116.92, 111.91, 110.49, 79.40, 70.40, 69.39, 49.03, 42.36, 40.52, 31.55, 28.51, 22.87.

Synthesis of tert-butyl (2-(2-(2-(2-((2-(2,6-dioxopiperidin-3-yl)-1,3-dioxoisoindolin-4- yl) a-mino)ethoxy)ethoxy)ethoxy) ethyl)carbamate (6c)

The synthesis of 6c followed the same procedure as 3a, replacing N-Boc-1,2-diaminoethane with 13-amino-5,8,11-trioxa-2-azatridecanoic acid 1,1-dimethylethyl ester. A green fluorescent powder was obtained, with a yield of 35.2%.[1]H NMR (500 MHz, Chloroform-d) δ 8.55 (s, 1H), 7.47 (dd, J = 8.5, 7.1 Hz, 1H), 7.09 (d, J = 7.0 Hz, 1H), 6.91 (d, J = 8.5 Hz, 1H), 6.48 (d, J = 5.4 Hz, 1H), 5.08 (d, J = 7.5 Hz, 1H), 4.91 (dd, J = 12.2, 5.4 Hz, 1H), 3.71 (t, J = 5.4 Hz, 2H), 3.66 (s, 4H), 3.64 – 3.62 (m, 2H), 3.61 – 3.58 (m, 2H), 3.52 (t, J = 5.3 Hz, 2H), 3.46 (q, J = 5.0 Hz, 2H), 3.29 (q, J = 5.2 Hz, 2H), 2.89 – 2.83 (m, 1H), 2.80 – 2.70 (m, 2H), 2.13 – 2.06 (m, 1H), 1.42 (s, 9H). [13]C NMR (126 MHz, $CDCl_3$) δ 171.40, 169.39, 168.62, 167.75, 156.18, 146.93, 136.15, 132.62, 116.90, 111.77, 110.40, 79.36, 70.85, 70.71, 70.69, 70.30, 69.60, 48.98, 42.49, 40.45, 31.54, 28.53, 22.89.

Intermediate 3a (1 g, 2.40 mmol) was dissolved in 10 mL of dichloromethane (DCM), and 2.5 mL of trifluoroacetic acid (TFA) was slowly added dropwise under ice bath conditions. The mixture was stirred at room temperature, and the reaction progress was monitored via TLC. Upon completion, the reaction mixture was concentrated under reduced pressure to remove DCM and TFA, yielding a yellow oily substance that required no further purification. After drying in a 40 °C oven, **Intermediate 4a** (a yellow fluorescent solid) was obtained with a 95% yield.

The synthesis methods of 4b-f and 7a-c followed the same procedure as 4a, requiring no further purification, and were used directly in the next step.

Synthesis of ((1R,2R,4aR,5R,8aS)-2-((4-((2-((2-(2,6-dioxopiperidin-3-yl)-1,3-dioxoisoindoli-n-4-yl)amino)ethyl)amino)-4-oxobutanoyl)oxy)-1,4a-dimethyl-6-methylene-5-((E)-2-(2-oxo-2,5-dihydrofuran-3-yl)vinyl)decahydronaphthalen-1-yl) methyl4-((2-((2-(2,6-dioxopiperidin-3-yl)-1,3-dioxoisoindolin-4-yl)amino)ethyl)amino)-4-oxobutanoate(DP_1)

PDS(1 eq, 1.75 mmol) and the intermediate 4a (2.5 eq,4.38 mmol) were firstly added to a 25 ml round bottom flask.Then the reaction mixture was added with 2 ml dry N, N-Dimethylformamide (DMF), N, N-Diisopropylethylamine (DIPEA, 3.0eq,5.26 mmol), 1-Hydroxybenzotriazo-le (HOBt, 3.0eq, 5.26 mmol) and 1-Ethyl-3-(3-dimethylaminopropyl)carbodiimide (EDCL,2eq, 3.5 mol). The mixture was stirred at room temperature for 12 h, and reaction progress was monitored by TLC. Upon completion, the ice-cold water was poured into reaction mixture with vigorous stirring, resulting in the precipitation of a yellow solid. The solid was collected by vacuum filtration, washed with cold water, and dried to yield a crude product, which was purified by preparative thin-layer chromatography (Dichloromethane: Methanol= 13: 1, v/v) to afford yellow solid powder DP_1 57 mg, with a yield of 28.9%. The compound DP_1 were structurally characterized using ^{1}H NMR, ^{13}C NMR, and HRMS analyses. ^{1}HNMR (500 MHz, Chloroform-d) δ 9.19 (d, J = 13.7 Hz, 2H), 7.44 (t, J = 7.9 Hz, 2H), 7.30 (t, J = 5.6 Hz, 1H), 7.16 (d, J = 8.0 Hz, 2H), 7.04 (t, J = 6.9 Hz, 2H), 6.87 (dd, J = 13.0, 6.5 Hz, 3H), 6.45 – 6.35 (m, 2H), 6.10 (d, J = 15.7 Hz, 1H), 4.96 – 4.88 (m, 2H), 4.79 (d, J = 11.9 Hz, 3H), 4.61 – 4.51 (m, 2H), 4.49 – 4.42 (m, 1H), 4.00 – 3.91 (m, 1H), 3.43 – 3.28 (m, 8H), 2.83 (d, J = 12.0 Hz,

2H), 2.74 (d, J = 10.9 Hz, 4H), 2.63 – 2.56 (m, 2H), 2.51 (q, J = 7.5, 6.5 Hz, 2H), 2.48 – 2.38 (m, 4H), 2.31 (d, J = 10.0 Hz, 2H), 2.11 – 2.05 (m, 2H), 2.01 (d, J = 10.7 Hz, 1H), 1.90 – 1.86 (m, 1H), 1.76 (d, J = 12.6 Hz, 1H), 1.63 (d, J = 9.8 Hz, 2H), 1.53 – 1.43 (m, 2H), 1.25 (d, J = 3.3 Hz, 1H), 0.97 (s, 3H), 0.81 (s, 3H).^{13}CNMR (126 MHz, Chloroform-d) δ 172.88, 172.77, 172.67, 172.32, 169.97, 169.86, 167.81, 148.02, 147.23, 143.79, 136.61, 135.81, 132.78, 129.46, 121.80, 117.11, 112.14, 110.27, 109.85, 80.59, 70.04, 64.41, 61.74, 55.23, 53.83, 49.28, 42.54, 42.26, 41.92, 38.86, 38.42, 36.80, 31.77, 31.04, 30.84, 30.38, 24.45, 23.65, 23.07, 22.85, 15.61. HRMS: calculated for $C_{58}H_{64}N_8O_{16}$ $[M+Na]^+$, 1151.4332; found, 1151.4337.

Synthesis of ((1R,2R,4aR,5R,8aS)-2-((4-((3-((2-(2,6-dioxopiperidin-3-yl)-1,3-dioxoisoindolin-4-yl)amino)propyl)amino)-4-oxobutanoyl)oxy)-1,4a-dimethyl-6-methylene-5-((E)-2-(2-oxo-2,5-dihydrofuran-3-yl)vinyl)decahydronaphthalen-1-yl) methyl 4-((3-((2-(2,6-dioxopiperidin-3-yl)- 1,3- dioxoisoindolin-4-yl)amino)propyl)amino)-4-oxobutanoate(DP_2)

The synthesis of DP_2 followed the same procedure as DP_1, replacing 3b with 3a.A yellow solid powder DP_2 61 mg,yield 30.1%. ^{1}H NMR (500 MHz, Chloroform-d) δ 9.09 (d, J = 5.7 Hz, 2H), 7.43 (t, J = 7.8 Hz, 2H), 7.17 (d, J = 2.2 Hz, 1H), 7.02 (d, J = 7.1 Hz, 2H), 6.86 (dd, J = 20.6, 9.3 Hz, 3H), 6.81 (s, 1H), 6.74 (d, J = 5.6 Hz, 1H), 6.37 (q, J = 5.4, 4.2 Hz, 2H), 6.10 (d, J = 15.8 Hz, 1H), 4.95 – 4.89 (m, 2H), 4.83 – 4.75 (m, 3H), 4.62 – 4.56 (m, 1H), 4.52 (s, 1H), 4.40 (d, J = 11.6 Hz, 1H), 4.03 (d, J = 11.6 Hz, 1H), 3.35 – 3.20 (m, 8H), 2.86 – 2.80 (m, 2H), 2.75 – 2.72 (m, 2H), 2.71 (s, 1H), 2.68 (t, J = 3.5 Hz, 1H), 2.63 – 2.56 (m, 2H), 2.53 – 2.47 (m, 2H), 2.46 – 2.41 (m, 2H), 2.31 (d, J = 10.0 Hz, 1H), 2.12 – 2.06 (m, 2H), 1.92 (s, 5H), 1.81 – 1.73 (m, 5H), 1.66 – 1.59 (m, 2H), 1.53 – 1.45 (m, 2H), 1.24 (s, 1H), 0.96 (s, 3H), 0.81 (s, 3H).^{13}CNMR (126 MHz, Chloroform-d) δ 172.73, 172.22, 172.10, 172.03, 171.76, 169.32, 169.05, 167.50, 147.56, 146.51, 143.33, 136.04, 135.31, 132.32, 128.93, 121.27, 116.56, 111.30, 109.75, 109.29, 77.13, 69.56, 64.13, 61.27, 54.68, 53.32, 48.75, 41.43, 39.82, 39.72, 38.37, 37.94, 36.87, 36.78, 36.33, 31.26, 30.67, 29.95, 29.74, 28.72, 23.97, 23.23, 22.63, 22.33, 15.11. HRMS: calculated for $C_{60}H_{68}N_8O_{16}$ $[M+Na]^+$, 1179.4645; found, 1179.4644.

Synthesis of ((1R,2R,4aR,5R,8aS)-2-((4-((4-((2-(2,6-dioxopiperidin-3-yl)-1,3-dioxoisoindolin-4-yl)amino) butyl) amino)-4-oxobutanoyl)oxy)-1,4a-dimethyl-6-methylene-5-((E)-2-(2-oxo-2,5-dihydrofuran-3-yl)vinyl)decahydronaphthalen-1-yl) methyl4-((4-((2-(2,6-dioxopiperidin-3-yl)- 1,3- dioxoisoindolin-4-yl)amino)butyl)amino)-4-oxobutanoate(DP_3)

The synthesis of DP_3 followed the same procedure as DP_1, replacing 3c with 3a.A yellow solid powder DP_3 60 mg,yield 29.1%.^{1}HNMR (500 MHz, Chloroform-d) δ 8.96 (d, J = 6.5 Hz, 2H), 7.46 (t, J = 7.8 Hz, 2H), 7.16 (d, J = 2.2 Hz, 1H), 7.05 (d, J = 7.1 Hz, 2H), 6.86 (dd, J = 11.9, 7.1 Hz, 3H), 6.71 (t, J = 5.5 Hz, 1H), 6.65 (t, J = 7.3 Hz, 1H), 6.27 – 6.19 (m, 2H), 6.10 (d, J = 15.8 Hz, 1H), 4.96 – 4.89 (m, 2H), 4.83 – 4.75 (m, 3H), 4.59 (dd, J = 11.0, 5.4 Hz, 1H), 4.53 (s, 1H), 4.39 (dd, J = 11.7, 3.4 Hz, 1H), 4.02 (d, J = 11.7 Hz, 1H), 3.23 (q, J = 7.7, 7.2 Hz, 5H), 3.17 (dd, J = 12.1, 6.2 Hz, 3H), 2.89 – 2.82 (m, 2H), 2.79 – 2.72 (m, 4H), 2.71 – 2.68 (m, 1H), 2.66 (dd, J = 7.3, 3.3 Hz, 1H), 2.63 – 2.59 (m, 1H), 2.57 (dd, J = 6.5, 3.7 Hz, 1H), 2.53 (s, 1H), 2.50 (q, J = 3.6 Hz, 1H), 2.47 – 2.39 (m, 3H), 2.31 (d, J = 10.0 Hz, 1H), 2.11 (t, J = 6.2 Hz, 2H), 2.06 – 1.97 (m, 2H), 1.89 (s, 4H), 1.75 (s, 1H), 1.66 – 1.58 (m, 6H), 1.56 – 1.46 (m, 6H), 1.31 – 1.27 (m, 1H), 1.25 (d, J = 6.2 Hz, 1H), 1.19 (d, J = 4.9 Hz, 1H), 0.97 (s, 3H), 0.81 (s, 3H).^{13}CNMR (126 MHz, Chloroform-d) δ 172.43, 172.35, 169.72, 169.48 – 169.02 (m), 147.79, 146.95, 143.55, 136.35, 135.56, 132.54, 129.19, 121.54, 116.88, 111.61, 109.89, 109.57, 80.31, 69.79, 64.34, 61.51, 54.97, 49.01, 42.26, 41.63, 39.10, 38.62, 38.18, 36.56, 31.52, 30.87, 30.26, 30.00, 26.94, 26.62, 23.44, 22.89, 22.58, 15.36. HRMS: calculated for $C_{62}H_{72}N_8O_{16}$ $[M+Na]^+$, 1207.4958; found, 1207.4962.

Synthesis of ((1R,2R,4aR,5R,8aS)-2-((4-((5-((2-(2,6-dioxopiperidin-3-yl)-1,3-dioxoisoindolin4- yl)amino)pentyl)amino)-4-oxobutanoyl)oxy)-1,4a-dimethyl-6-methylene-5-((E)-2-(2-oxo-2,5-di-hydrofuran-3- yl)vinyl) decahydronaphthalen-1-yl)methyl 4-((5-((2-(2,6-dioxopiperidin-3-yl)-1,3-dioxoisoindolin-4-yl)amino) pentyl) amino)-4-oxobutanoate(DP_4)

The synthesis of DP_4 followed the same procedure as DP_1, replacing 3 d with 3a.A yellow solid powder DP_4 66 mg,yield 31.3%.^{1}H NMR (500 MHz, Chloroform-d) δ 8.85 (d, J = 8.2 Hz, 2H), 7.47 (t, J = 7.8 Hz, 2H), 7.16 (d, J = 2.4 Hz, 1H), 7.06 (d, J = 7.0 Hz, 2H), 6.91 – 6.83 (m, 3H), 6.56 – 6.49 (m, 1H), 6.43 (dd, J = 20.5, 5.7 Hz, 1H), 6.23 (q, J = 6.3 Hz, 2H), 6.10 (d, J = 15.7 Hz, 1H), 4.95 – 4.89 (m, 2H), 4.82 – 4.76 (m, 3H), 4.59 (dd, J = 10.7, 5.7 Hz, 1H), 4.53 (s, 1H), 4.40 (d, J = 11.7 Hz, 1H), 4.03 (d, J = 11.7 Hz, 1H), 3.24 (q, J = 6.4 Hz, 5H), 3.21 – 3.15 (m, 3H), 2.89 – 2.83 (m, 2H), 2.78 – 2.72 (m, 4H), 2.68 (d, J = 3.2 Hz, 1H), 2.63 (t, J = 7.3 Hz, 1H), 2.60 – 2.57 (m, 1H), 2.55 – 2.52 (m, 1H), 2.50 (d, J = 6.8 Hz, 1H), 2.46 (d, J = 8.1 Hz, 1H), 2.44 – 2.42 (m, 1H), 2.31 (d, J = 10.0 Hz, 1H), 2.11 (q, J = 7.1, 6.7 Hz, 2H), 2.04 – 1.98 (m, 2H), 1.96 – 1.89 (m, 2H), 1.78 (d, J = 12.8 Hz, 2H), 1.67 – 1.60 (m, 6H), 1.52 – 1.47 (m, 5H), 1.43 – 1.37 (m, 4H), 1.24 (s, 1H), 0.98 (s, 3H), 0.82 (s, 3H).^{13}CNMR (126 MHz, Chloroform-d) δ 172.49, 172.42, 171.79, 171.74, 171.68, 169.72, 169.07, 167.75, 147.81, 147.02, 143.53, 136.31, 135.57, 132.56, 129.21, 121.53, 116.85, 111.57, 109.94, 109.54, 80.37, 69.78, 64.44, 61.54, 54.97, 49.00, 42.47, 41.63, 39.40, 38.64, 38.20, 36.59, 31.52, 30.96, 30.27,

30.07, 29.81, 29.18, 28.73, 24.20, 23.51, 22.91, 22.58, 15.36. HRMS: calculated for $C_{64}H_{76}N_8O_{16}$ $[M+Na]^+$, 1235.5271; found, 1235.5273.

Synthesis of ((1R,2R,4aR,5R,8aS)-2-((4-((6-((2-(2,6-dioxopiperidin-3-yl)-1,3-dioxoisoindolin-4-yl)amino)hexyl) amino)-4-oxobutanoyl)oxy)-1,4a-dimethyl-6-methylene-5-((E)-2-(2-oxo-2,5-dihydrofuran-3-yl)vinyl)decahydronaphthalen-1-yl)methyl 4-((6-((2-(2,6-dioxopiperidin-3-yl)-1,3-dioxoisoindolin-4-yl)amino)hexyl)amino)-4-oxobutanoate(DP_5)

The synthesis of DP_5 followed the same procedure as DP_1, replacing 3e with 3a.A yellow solid powder DP_5 75 mg,yield 34.5%.^{1}H NMR (500 MHz, Chloroform-d) δ 8.70 (d, J = 12.4 Hz, 2H), 7.47 (t, J = 7.9 Hz, 2H), 7.16 (s, 1H), 7.07 (d, J = 7.1 Hz, 2H), 6.86 (d, J = 9.2 Hz, 3H), 6.37 (d, J = 53.3 Hz, 2H), 6.21 (s, 2H), 6.10 (d, J = 15.7 Hz, 1H), 4.92 (t, J = 8.1 Hz, 2H), 4.79 (d, J = 10.9 Hz, 3H), 4.60 (t, J = 8.2 Hz, 1H), 4.53 (s, 1H), 4.39 (d, J = 11.8 Hz, 1H), 4.05 (d, J = 11.8 Hz, 1H), 3.29 – 3.13 (m, 8H), 2.86 (d, J = 13.7 Hz, 2H), 2.75 (q, J = 9.6, 5.4 Hz, 4H), 2.71 – 2.65 (m, 2H), 2.61 (d, J = 21.0 Hz, 2H), 2.54 (d, J = 8.2 Hz, 1H), 2.49 (dd, J = 16.2, 8.1 Hz, 2H), 2.45 – 2.39 (m, 2H), 2.31 (d, J = 10.0 Hz, 1H), 2.12 (d, J = 9.8 Hz, 2H), 2.01 (t, J = 12.7 Hz, 2H), 1.81 (s, 1H), 1.65 – 1.58 (m, 5H), 1.51 – 1.44 (m, 5H), 1.42 – 1.37 (m, 4H), 1.35 – 1.29 (m, 4H), 1.24 (s, 3H), 0.98 (s, 3H), 0.83 (s, 3H).^{13}CNMR (126 MHz, Chloroform-d) δ 172.68, 172.21, 172.14, 171.41, 171.35, 171.27, 169.46, 168.63, 167.50, 147.57, 146.82, 143.23, 136.05, 135.35, 132.32, 128.97, 121.27, 116.60, 111.30, 109.68, 109.30, 80.09, 69.51, 64.21, 61.31, 54.73, 48.74, 42.35, 41.39, 39.32, 38.40, 37.97, 36.36, 31.27, 30.78, 30.01, 29.81, 29.56, 29.22, 28.84, 26.46, 26.39, 23.97, 23.28, 22.68, 22.35, 15.12. HRMS: calculated for $C_{66}H_{80}N_8O_{16}$ $[M+H]^+$, 1241.5765; found, 1241.5769.

Synthesis of

((1R,2R,4aR,5R,8aS)-2-((4-((8-((2-(2,6-dioxopiperidin-3-yl)-1,3-dioxoisoindolin-4-yl)amino)octyl)amino)-4-oxobutanoyl)oxy)-1,4a-dimethyl-6-methylene-5-((E)-2-(2-oxo-2,5-dih-ydrofuran-3-yl)vinyl)decahydronaphthalen-1-yl)methyl4-((8-((2-(2,6-dioxopiperidin-3-yl)-1,3-d-ioxoisoindolin-4-yl)amino)octyl)amino)-4-oxobutanoate(DP_6)

The synthesis of DP_6 followed the same procedure as DP_1, replacing 3 f with 3a.A yellow solid powder DP_6 74 mg,yield 32.7%.^{1}H NMR (500 MHz, Chloroform-d) δ 8.64 (d, J = 7.1 Hz, 2H), 7.51 – 7.44 (m, 2H), 7.16 (s, 1H), 7.07 (s, 2H), 6.88 (dd, J = 16.7, 9.3 Hz, 3H), 6.22 (t, J = 5.5 Hz, 2H), 6.10 (d, J = 15.8 Hz, 1H), 4.91 (dd, J = 12.0, 5.4 Hz, 2H), 4.79 (dd, J = 8.3, 2.0 Hz, 3H), 4.61 (dd, J = 9.9, 6.4 Hz, 1H), 4.53 (d, J = 1.9 Hz, 1H), 4.39 (d, J = 11.6 Hz, 1H), 4.06 (d, J = 11.7 Hz, 1H), 3.24 (q, J = 6.6 Hz, 4H), 3.21 – 3.12 (m, 4H), 2.90 – 2.83 (m, 2H), 2.82 – 2.77 (m, 1H), 2.76 – 2.62 (m, 6H), 2.62 – 2.57 (m, 1H), 2.53 – 2.48 (m, 2H), 2.47 – 2.38 (m, 3H), 2.32 (d, J = 10.1 Hz, 1H), 2.14 – 2.09 (m, 2H), 2.05 – 1.99 (m, 1H), 1.84 – 1.76 (m, 4H), 1.67 – 1.60 (m, 6H), 1.55 – 1.49 (m, 2H), 1.47 – 1.43 (m, 3H), 1.37 (d, J = 7.9 Hz, 3H), 1.33 – 1.30 (m, 3H), 1.30 – 1.26 (m, 9H), 1.24 (d, J = 3.3 Hz, 1H), 0.99 (s, 3H), 0.83 (s, 3H).^{13}CNMR (126 MHz, Chloroform-d) δ 172.93, 172.48, 172.38, 171.59, 171.52, 171.47, 169.67, 168.81, 168.79, 167.77, 147.83, 147.10, 143.46, 136.25, 135.62, 132.58, 129.23, 121.51, 116.81, 111.48, 109.90, 109.54, 80.34, 69.76, 64.46, 61.58, 54.99, 53.57, 48.98, 42.66, 41.64, 39.75, 38.66, 38.23, 36.62, 31.53, 31.07, 30.27, 30.09, 29.58, 29.21, 29.19, 29.15, 26.86, 26.83, 24.22, 23.55, 22.93, 22.60, 15.37. HRMS: calculated for $C_{70}H_{88}N_8O_{16}$ $[M+Na]^+$, 1319.6210; found, 1319.6212.

Synthesis of ((1R,2R,4aR,5R,8aS)-2-((4-((2-(2-((2-(2,6-dioxopiperidin-3-yl)-1,3-dioxoisoindoli-n-4-yl)amino) ethoxy)ethyl)amino)-4-oxobutanoyl)oxy)-1,4a-dimethyl-6-methylene-5-((E)-2-(2-oxo-2,5-dihydrofuran-3-yl)vinyl) decahydronaphthalen-1-yl)methyl 4-((2-(2-((2-(2,6-dioxopiper-idin-3-yl)-1,3-dioxoisoindolin-4-yl)amino) ethoxy)ethyl)amino)-4-oxobutanoate(DP_7)

The synthesis of DP_7 followed the same procedure as DP_1, replacing 5a with 3a.A yellow solid powder DP_7 75 mg,yield 35.2%.^{1}H NMR (500 MHz, Chloroform-d) δ 9.41 – 8.99 (m, 2H), 7.49 (t, J = 7.8 Hz, 2H), 7.17 (s, 1H), 7.09 (d, J = 7.1 Hz, 2H), 6.87 (q, J = 9.0 Hz, 3H), 6.77 – 6.71 (m, 1H), 6.68 – 6.59 (m, 3H), 6.12 (d, J = 15.8 Hz, 1H), 5.06 – 4.94 (m, 2H), 4.79 (d, J = 13.9 Hz, 3H), 4.54 (d, J = 6.9 Hz, 2H), 4.43 – 4.34 (m, 1H), 4.07 – 3.99 (m, 1H), 3.69 (p, J = 5.0 Hz, 4H), 3.56 (p, J = 9.7, 4.8 Hz, 5H), 3.47 (t, J = 5.3 Hz, 2H), 3.43 – 3.38 (m, 5H), 2.84 – 2.74 (m, 6H), 2.66 (d, J = 7.4 Hz, 3H), 2.60 – 2.51 (m, 5H), 2.43 (d, J = 13.4 Hz, 1H), 2.32 (d, J = 10.2 Hz, 1H), 2.10 (d, J = 7.5 Hz, 2H), 2.03 (s, 1H), 2.01 – 1.97 (m, 1H), 1.80 – 1.75 (m, 1H), 1.64 (d, J = 9.3 Hz, 2H), 1.54 – 1.48 (m, 2H), 1.24 (s, 2H), 0.97 (s, 3H), 0.83 (s, 3H).^{13}C NMR (126 MHz, Chloroform-d) δ 173.02, 172.15, 171.76, 169.65, 168.82, 167.45, 147.77, 146.66, 146.63, 143.14, 136.12, 135.44, 132.29, 129.03, 121.19, 116.74, 111.69, 110.25, 109.11, 80.19, 69.75, 69.50, 68.35, 64.43, 61.35, 54.57, 48.74, 41.75, 41.32, 39.13, 38.46, 37.96, 36.48, 31.22, 30.44, 29.55, 22.69, 15.03. HRMS: calculated for $C_{62}H_{72}N_8O_{18}$ $[M+H]^+$, 1217.5037; found, 1217.5041.

Synthesis of (1R,2R,4aR,5R,8aS)-1-(15-((2-(2,6-dioxopiperidin-3-yl)-1,3-dioxoisoindolin-4-yl) amino)-3,6-dioxo-2,10,13-trioxa-7-azapentadecyl)-1,4a-dimethyl-6-

methylene-5-((E)-2-(2-oxo-2,5-dihydrofuran-3-yl)vinyl) decahydronaphthalen-2-yl 4-((2-(2-(2-((2-(2,6-dioxopiperidin-3-yl)-1,3-dioxoisoindolin-4-yl)amino)ethoxy) ethoxy)ethyl)amino)-4-oxobutanoate(DP_8)

The synthesis of DP_8 followed the same procedure as DP_1, replacing 5b with 3a.A yellow solid powder DP_8 77 mg,yield 33.7%.^{1}H NMR (500 MHz, Chloroform-d) δ 9.30 – 9.06 (m, 2H), 7.48 (t, J = 7.8 Hz, 2H), 7.16 (s, 1H), 7.08 (d, J = 7.1 Hz, 2H), 6.89 (d, J = 8.7 Hz, 2H), 6.86 (d, J = 10.0 Hz, 1H), 6.78 – 6.71 (m, 1H), 6.69 (q, J = 6.0 Hz, 1H), 6.52 (t, J = 5.3 Hz, 2H), 6.10 (d, J = 15.7 Hz, 1H), 4.98 – 4.90 (m, 2H), 4.78 (d, J = 13.4 Hz, 3H), 4.59 – 4.50 (m, 2H), 4.35 (dd, J = 11.8, 3.2 Hz, 1H), 4.07 (d, J = 11.7 Hz, 1H), 3.72 (q, J = 4.5 Hz, 4H), 3.66 – 3.60 (m, 8H), 3.54 (q, J = 5.5 Hz, 4H), 3.45 (d, J = 5.5 Hz, 3H), 3.41 – 3.38 (m, 3H), 2.84 (d, J = 3.5 Hz, 1H), 2.82 – 2.80 (m, 1H), 2.80 – 2.77 (m, 1H), 2.74 (d, J = 11.0 Hz, 3H), 2.65 – 2.60 (m, 3H), 2.57 (d, J = 5.4 Hz, 1H), 2.48 – 2.43 (m, 4H), 2.41 (d, J = 5.6 Hz, 1H), 2.31 (d, J = 10.2 Hz, 2H), 2.12 – 2.06 (m, 3H), 2.00 (q, J = 11.4, 10.4 Hz, 2H), 1.78 (d, J = 13.2 Hz, 1H), 1.61 (d, J = 12.3 Hz, 2H), 1.50 (dd, J = 13.6, 4.1 Hz, 2H), 0.97 (s, 3H), 0.83 (s, 3H).^{13}CNMR (126 MHz, Chloroform-d) δ 172.85, 172.65, 172.19, 172.11, 169.84, 169.39, 168.01, 148.24, 147.07, 143.66, 136.49, 135.94, 132.89, 129.50, 121.70, 117.14, 112.07, 110.67, 110.64, 109.64, 80.57, 70.88, 70.39, 70.23, 70.01, 69.46, 64.95, 61.87, 55.12, 49.24, 42.58, 41.84, 39.72, 38.93, 38.49, 36.95, 31.73, 31.06, 31.00, 30.26, 29.99, 29.67, 24.42, 23.96, 23.21, 22.89, 15.57. HRMS: calculated for $C_{66}H_{80}N_8O_{20}$ $[M+Na]^+$, 1327.5381; found, 1327.5386.

Synthesis of ((1R,2R,4aR,5R,8aS)-2-((1-((2-(2,6-dioxopiperidin-3-yl)-1,3-dioxoisoindolin-4-yl)amino)-13-oxo-3,6,9-trioxa-12-azahexadecan-16-oyl)oxy)-1,4a-dimethyl-6-methylene-5-((E)-2-(2-oxo-2,5-dihydrofuran-3-yl)vinyl)decahydronaphthalen-1-yl)methyl1-((2-(2,6-dioxopiperi-din-3-yl)-1,3-dioxoisoindolin-4-yl)amino)-13-oxo-3,6,9-trioxa-12-azahexadecan-16-oate(DP9)

The synthesis of DP_9 followed the same procedure as DP_1, replacing 5c with 3a.A yellow solid powder DP_9 73 mg,yield 29.9%.^{1}H NMR (500 MHz, Chloroform-d) δ 8.98 (d, J = 5.2 Hz, 2H), 7.48 (t, J = 7.8 Hz, 2H), 7.16 (s, 1H), 7.08 (d, J = 7.2 Hz, 2H), 6.89 (dd, J = 12.9, 6.9 Hz, 3H), 6.82 (d, J = 5.2 Hz, 1H), 6.76 (s, 1H), 6.49 (t, J = 5.6 Hz, 2H), 6.10 (d, J = 15.8 Hz, 1H), 4.99 – 4.89 (m, 2H), 4.79 (d, J = 13.7 Hz, 3H), 4.55 (d, J = 23.5 Hz, 2H), 4.35 (d, J = 11.7 Hz, 1H), 4.09 (d, J = 11.7 Hz, 1H), 3.72 (t, J = 5.2 Hz, 4H), 3.66 (s, 7H), 3.64 – 3.62 (m, 3H), 3.61 – 3.57 (m, 4H), 3.52 (q, J = 5.5 Hz, 4H), 3.46 (q, J = 5.5 Hz, 4H), 3.39 (q, J = 5.0 Hz, 3H), 2.87 – 2.81 (m, 2H), 2.79 – 2.71 (m, 4H), 2.67 – 2.61 (m, 3H), 2.59 – 2.52 (m, 2H), 2.51 – 2.44 (m, 4H), 2.42 (d, J = 4.6 Hz, 1H), 2.31 (d, J = 10.0 Hz, 1H), 2.14 – 2.06 (m, 5H), 2.00 (d, J = 4.6 Hz, 1H), 1.79 (d, J = 12.1 Hz, 1H), 1.66 – 1.60 (m, 2H), 1.51 (dd, J = 14.0, 4.6 Hz, 2H), 1.24 (s, 1H), 0.97 (s, 3H), 0.83 (s, 3H).^{13}CNMR (126 MHz, Chloroform-d) δ 173.29, 172.80, 172.65, 172.15, 172.09, 172.02, 169.71, 169.21, 168.03, 148.23, 147.13, 143.67, 136.45, 135.94, 132.88, 129.50, 121.72, 117.17, 112.03, 110.63, 109.66, 80.55, 71.07, 70.89, 70.80, 70.48, 70.13, 70.01, 69.73, 64.95, 61.90, 55.15, 49.24, 42.69, 41.85, 39.66, 38.95, 38.51, 36.96, 31.79, 31.04, 30.29, 30.06, 24.44, 23.99, 23.16, 22.90, 15.59. HRMS: calculated for $C_{70}H_{88}N_8O_{22}$ $[M+Na]^+$, 1415.5905; found, 1415.5910.

Synthesis of DL_1 PROTAC

Synthesis of tert-butyl (9-((2-(2,6-dioxopiperidin-3-yl)-1-oxoisoindolin-4-yl)amino)-9-oxonon-yl)carbamate(9)

To a solution of 9-((tert-butoxycarbonyl)amino)nonanoic acid (1.2eq,3.66 mmol) in dry DMF (2.0 mL), DIPEA (2.0 eq, 8.16 mmol) was slowly added and stirred at room temperature for 5 min,then (HATU) (1.5eq,4.56 mmol) was added. The reaction progress was monitored via TLC for about 0.5 h. Then the reaction mixture was added with L-DOPA (1.0eq,3.05 mmol) .The reaction was allowed to stir at room temperature for approximately 12 h. with reaction progress monitored by TLC. Upon completion, the reaction was quenched with ice water, and the mixture was extracted with ethyl acetate. The organic layers were combined, washed with saturated $NaHCO_3$ and brine, dried over anhydrous Na_2SO_4, filtered, and concentrated under reduced pressure. The crude product was purified by silica gel column chromatography (DCM:MeOH=20:1), yielding a white solid powder (intermediate 9), with a yield of 67.3%.^{1}HNMR (500 MHz, DMSO-d6) δ 11.02 (s, 1H), 9.78 (s, 1H), 7.80 (d, J = 7.4 Hz, 1H), 7.48 (q, J = 7.5 Hz, 2H), 6.75 (s, 1H), 5.74 (s, 2H), 5.14 (dd, J = 13.3, 5.1 Hz, 1H), 4.40 – 4.30 (m, 2H), 2.88 (t, J = 6.5 Hz, 2H), 2.62 (s, 1H), 2.36 – 2.32 (m, 2H), 2.06 – 1.98 (m, 1H), 1.59 (t, J = 7.2 Hz, 2H), 1.36 (s, 9H), 1.29 (d, J = 3.5 Hz, 2H), 1.27 (s, 2H), 1.26 (s, 2H), 1.25 (s, 2H), 1.23 (s, 2H).^{13}CNMR (126 MHz, DMSO-d6) δ 173.32, 171.87, 171.52, 168.33, 156.06, 134.28, 134.15, 133.12, 129.06, 125.71, 119.42, 77.75, 55.33, 52.00, 49.05, 46.96, 36.25, 31.66, 29.92, 29.12, 28.95, 28.70, 26.66, 25.51, 23.10.

Intermediate 9 (1 g, 1.94 mmol) was dissolved in 10 mL of dichloromethane (DCM), and 2.5 mL of trifluoroacetic acid (TFA) was slowly added dropwise under ice bath conditions. The mixture was stirred at room temperature, and the reaction progress was monitored via TLC. Upon completion, the reaction mixture was concentrated under reduced pressure to remove DCM and TFA, yielding a white oily substance that required no further purification.

After drying in a 40 °C oven, **Intermediate 10**(a white solid powder) was obtained with a 95% yield.

Synthesis of ((1R,2R,4aR,5R,8aS)-2-((4-((9-((2-(2,6-dioxopiperidin-3-yl)-1-oxoisoindolin-4-yl) amino)-9-oxononyl) amino)-4-oxobutanoyl)oxy)-1,4a-dimethyl-6-methylene-5-((E)-2-(2-oxo-2, 5-dihydrofu-ran-3-yl)vinyl) decahydronaphthalen-1-yl)methyl 4-((9-((2-(2,6-dioxopiperidin-3-yl)-1-oxoisoind-olin-4-yl)amino)-9-oxononyl)amino)-4-oxobutanoate(DL_1)

PDS(1 eq,1.75 mmol) and the intermediate 10 (2.5 eq,4.38 mmol) were fistly added to a 25 ml round bottom flask.Then the reaction mixture was added with 2 ml dry DMF, DIPEA (3.0eq,5.26 mmol)and HOBt (3.0eq, 5.26 mmol). After completing the above experimental procedure, the reaction was stirred at room temperature for 12 h. The progress of the reaction was monitored by TLC. After the reaction was completed, the reaction mixture was concentrated under reduced pressure to give a crude material, which was purified by preparative thin-layer chromatography (Dichloromethane: Methanol= 13: 1, v/v) to afford yellow solid powder DL_1 76 mg, with a yield of 32.9%.^{1}H NMR (500 MHz, DMSO-d6) δ 11.02 (s, 2H), 9.76 (s, 2H), 7.85 – 7.78 (m, 4H), 7.64 (d, J = 2.0 Hz, 1H), 7.51 – 7.45 (m, 4H), 6.74 (dd, J = 15.8, 10.1 Hz, 1H), 6.14 (d, J = 15.8 Hz, 1H), 5.13 (dd, J = 13.3, 5.2 Hz, 2H), 4.92 – 4.86 (m, 2H), 4.74 (s, 1H), 4.51 (dd, J = 11.9, 4.5 Hz, 1H), 4.43 (s, 1H), 4.40 – 4.29 (m, 4H), 4.21 (d, J = 11.6 Hz, 1H), 4.10 (d, J = 11.7 Hz, 1H), 3.04 – 2.96 (m, 4H), 2.91 (ddd, J = 17.9, 13.7, 5.5 Hz, 2H), 2.64 – 2.57 (m, 2H), 2.47 – 2.42 (m, 2H), 2.38 – 2.27 (m, 11H), 2.10 – 1.91 (m, 4H), 1.76 (s, 1H), 1.59 (q, J = 7.4 Hz, 5H), 1.41 (s, 1H), 1.35 (q, J = 6.3 Hz, 5H), 1.32 – 1.26 (m, 8H), 1.23 (q, J = 9.3, 7.0 Hz, 13H), 0.93 (s, 3H), 0.77 (s, 3H). ^{13}C NMR (126 MHz, DMSO-d6) δ 173.40, 172.95, 172.72, 172.38, 171.93, 171.60, 170.94, 168.39, 149.06, 147.53, 134.33, 134.18, 133.18, 129.15, 127.59, 125.75, 122.09, 119.50, 108.86, 79.68, 70.73, 64.55, 60.58, 53.78, 52.07, 47.01, 41.54, 39.05, 38.69, 38.05, 36.60, 36.34, 31.73, 30.38, 30.30, 29.86, 29.78, 29.64, 29.54, 29.30, 29.22, 29.19, 26.93, 26.90, 25.62, 24.25, 23.96, 23.17, 22.67, 15.28. HRMS: calculated for $C_{72}H_{92}N_8O_{16}$ $[M+Na]^+$, 1347.6524; found, 1347.6528.

In silico ADME prediction

The physicochemical and pharmacokinetic properties of representative PROTAC compounds (DP1–DP7, DL1, and SP6) were predicted using the SwissADME web tool (http://www.swissadme.ch), a free-access platform developed by the Swiss Institute of Bioinformatics. Canonical SMILES strings of each compound were input into the system to calculate molecular descriptors, including molecular weight (MW), topological polar surface area (TPSA), number of rotatable bonds, hydrogen-bond donors and acceptors, and lipophilicity (logP). Drug-likeness evaluations were based on Lipinski's rule of five, Ghose, Veber, Egan, and Muegge criteria. Bioavailability scores, PAINS alerts, synthetic accessibility indices, and predicted solubility (LogS) values were also obtained. The tool was used in April 2025 with default settings.

Data Availability

Data will be made available on request.

Supplementary information The online version contains supplementary material available at https://doi.org/10.1007/s00044-025-03434-0.

Acknowledgements This study received funding from the Fujian Provincial Education Department for young and middle-aged teachers (Grant No.JAT241353), Key Science and Technology Projects of Quanzhou Medical College (Grant No. XJK2211A), the QuanZhou High Level Talent Innovation and Entrepreneurship Project (Grant No. 2023C003R), and the National Natural Science Foundation of China (Grant No. 21772047). We would also like to acknowledge the Instrumental Analysis Center of HUAQIAO UNIVERSITY for their support in conducting NMR experiments.

Author contributions RL.S. and M.C. wrote the main manuscript text, RL.S. was mainly responsible for synthesizing the compounds and J.H. Y.W. YR.L. assisted in the synthesis of the compounds, PX.Z. WM.L. HG.Z. and M.X. were mainly responsible for the cellular activity assay and the western blot experiments, JQ. L. was responsible for review and coordination. All authors reviewed the manuscript.

Compliance with ethical standards

Conflict of interest The authors declare no competing.

References

1. Upadhyay A. Cancer: an unknown territory; rethinking before going ahead. Genes Dis. 2021;8:655–61.
2. Han B, Zheng R, Zeng H, Wang S, Sun K, Chen R, et al. Cancer incidence and mortality in China, 2022. J Natl Cancer Cent. 2024;4:47–53.
3. Gharwan H, Groninger H. Kinase inhibitors and monoclonal antibodies in oncology: clinical implications. Nat Rev Clin Oncol. 2015;13:209–27.
4. Cromm PM, Crews CM. Targeted protein degradation: from chemical biology to drug discovery. Cell Chem Biol. 2017;24:1181–90.
5. Bekes M, Langley DR, Crews CM. PROTAC targeted protein degraders: the past is prologue. Nat Rev Drug Discov. 2022;21:181–200.
6. Dale B, Cheng M, Park KS, Kaniskan HÜ, Xiong Y, Jin J. Advancing targeted protein degradation for cancer therapy. Nat Rev Cancer. 2021;21:638–54.
7. Li K, Crews CM. PROTACs: past, present and future. Chem Soc Rev. 2022;51:5214–36.
8. Li X, Pu W, Zheng Q, Ai M, Chen S, Peng Y. Proteolysis-targeting chimeras (PROTACs) in cancer therapy. Mol Cancer. 2022;21:99.
9. Salerno A, Seghetti F, Caciolla J, Uliassi E, Testi E, Guardigni M, et al. Enriching proteolysis targeting chimeras with a second

modality: when two are better than one. J Med Chem. 2022;65:9507–30.
10. Gadd MS, Testa A, Lucas X, Chan KH, Chen W, Lamont DJ, et al. Structural basis of PROTAC cooperative recognition for selective protein degradation. Nat Chem Biol. 2017;13:514–21.
11. Zhao L, Zhao J, Zhong K, Tong A, Jia D. Targeted protein degradation: mechanisms, strategies and application. Signal Transduct Target Ther. 2022;7:113.
12. Smith BE, Wang SL, Jaime-Figueroa S, Harbin A, Wang J, Hamman BD, et al. Differential PROTAC substrate specificity dictated by orientation of recruited E3 ligase. Nat Commun. 2019;10:131.
13. Qi Z, Yang G, Deng T, Wang J, Zhou H, Popov SA, et al. Design and linkage optimization of ursane-thalidomide-based PROTACs and identification of their targeted-degradation properties to MDM2 protein. Bioorganic Chem. 2021;111:104901.
14. Burslem GM, Song J, Chen X, Hines J, Crews CM. Enhancing antiproliferative activity and selectivity of a FLT-3 inhibitor by proteolysis targeting chimera conversion. J Am Chem Soc. 2018;140:16428–32.
15. Li X, Yao Y, Wu F, Song Y. A proteolysis-targeting chimera molecule selectively degrades ENL and inhibits malignant gene expression and tumor growth. J Hematol Oncol. 2022;15:41.
16. Li X, Yuan W, Wu J, Zhen J, Sun Q, Yu M. Andrographolide, a natural anti-inflammatory agent: an update. Front Pharmacol. 2022;13:920435.
17. Sharma V, Sharma T, Kaul S, Kapoor KK, Dhar MK. Anticancer potential of labdane diterpenoid lactone "andrographolide" and its derivatives: a semi-synthetic approach. Phytochemistry Rev. 2016;16:513–26.
18. Kaewpiboon C, Boonnak N, Salae AW, Pakdeepromma S, Yawut N, Chung YH. Andrographolide targets EGFR to impede epithelial–mesenchymal transition in human breast cancer cells. J Pharm Biomed Anal. 2024;248:116267.
19. Yu X, Xu J, Cahuzac KM, Xie L, Shen Y, Chen X, et al. Novel allosteric inhibitor-derived akt proteolysis targeting chimeras (PROTACs) enable potent and selective AKT degradation in KRAS/BRAF mutant cells. J Med Chem. 2022;65:14237–60.
20. Peng Y, Li J, Sun Y, Chan JYW, Sheng D, Wang K, et al. SAR studies of 3,14,19-derivatives of andrographolide on anti-proliferative activity to cancer cells and toxicity to zebrafish: an in vitro and in vivo study. RSC Adv. 2015;5:22510–26.
21. Xu H, Zhang H, Wu Y, Liu Y, Li X, Wang J. et al. The network pharmacology and molecular docking analysis on the anti-tumor effects of andrographolide. Chin J Hosp Pharm. 2020;40:1312–9.
22. Eskandari E, Negri GL, Tan S, MacAldaz ME, Ding S, Long J, et al. Dependence of human cell survival and proliferation on the CASP3 prodomain. Cell Death Discov. 2024;10:63.
23. Zheng M, Huo J, Gu X, Wang Y, Wu C, Zhang Q, et al. Rational design and synthesis of novel dual PROTACs for simultaneous degradation of EGFR and PARP. J Med Chem. 2021;64:7839–52.
24. Hines J, Lartigue S, Dong H, Qian Y, Crews CM. MDM2-Recruiting PROTAC offers superior, synergistic antiproliferative activity via simultaneous degradation of BRD4 and stabilization of p53. Cancer Res. 2019;79:251–62.
25. Dong Y, Ma T, Xu T, Feng Z, Li Y, Song L, et al. Characteristic roadmap of linker governs the rational design of PROTACs. Acta Pharm Sin B. 2024;14:4266–95.
26. Zhu Y, Ye X, Wu Y, Shen H, Cai Z, Xia F, et al. Design, synthesis, and biological evaluation of novel EGFR PROTACs targeting C797S mutation. J Med Chem. 2024;67:7283–7300.
27. Han X, Zhao L, Xiang W, Qin C, Miao B, McEachern D, et al. Strategies toward discovery of potent and orally bioavailable proteolysis targeting chimera degraders of androgen receptor for the treatment of prostate cancer. J Med Chem. 2021;64:12831–54.
28. Mi D, Li Y, Gu H, Li Y, Chen Y. Current advances of small molecule E3 ligands for proteolysis-targeting chimeras design. Eur J Med Chem. 2023;256:115444.
29. Xiang W, Zhao L, Han X, Qin C, Miao B, McEachern D, et al. Discovery of ARD-2585 as an exceptionally potent and orally active PROTAC degrader of androgen receptor for the treatment of advanced prostate cancer. J Med Chem. 2021;64:13487–509.
30. Bricelj A, Dora Ng YL, Ferber D, Kuchta R, Müller S, Monschke M, et al. Influence of linker attachment points on the stability and neosubstrate degradation of cereblon ligands. ACS Med Chem Lett. 2021;12:1733–8.
31. Zhang X, Zhao T, Sun M, Li P, Lai M, Xie L, et al. Design, synthesis and biological evaluation of KRASG12C-PROTACs. Bioorganic Medicinal Chem. 2023;78:117153.
32. Zhou H, Bai L, Xu R, Zhao Y, Chen J, McEachern D, et al. Structure-based discovery of SD-36 as a potent, selective, and efficacious PROTAC degrader of STAT3 protein. J Med Chem. 2019;62:11280–11300.
33. Fu X, Mao Q, Zhang B, Lv J, Ping K, Zhang P, et al. Thiazolidinedione-based structure modification of celastrol provides thiazolidinedione-conjugated derivatives as potent agents against non-small-cell lung cancer cells through a mitochondria-mediated apoptotic pathway. J Nat Products. 2022;85:1147–56.
34. Guenette RG, Yang SW, Min J, Pei B, Potts PR. Target and tissue selectivity of PROTAC degraders. Chem Soc Rev. 2022;51:5740–56.
35. Liu Z, Hu M, Yang Y, Du C, Zhou H, Liu C, et al. An overview of PROTACs: a promising drug discovery paradigm. Mol Biomed. 2022;3:46.
36. Zhao C, Chen D, Suo F, Setroikromo R, Quax WJ, Dekker FJ. Discovery of highly potent HDAC8 PROTACs with anti-tumor activity. Bioorganic Chem. 2023;136:106546.
37. Xue C, Yao Q, Gu X, Shi Q, Yuan X, Chu Q, et al. Evolving cognition of the JAK-STAT signaling pathway: autoimmune disorders and cancer. Signal Transduct Target Ther. 2023;8:204.
38. Daina A, Michielin O, Zoete V. SwissADME: a free web tool to evaluate pharmacokinetics, drug-likeness and medicinal chemistry friendliness of small molecules. Sci Rep. 2017;7:42717.

Publisher's note Springer Nature remains neutral with regard to jurisdictional claims in published maps and institutional affiliations.

Springer Nature or its licensor (e.g. a society or other partner) holds exclusive rights to this article under a publishing agreement with the author(s) or other rightsholder(s); author self-archiving of the accepted manuscript version of this article is solely governed by the terms of such publishing agreement and applicable law.